The activation mechanism of $\alpha_1\beta_2\gamma_{2S}$ and $\alpha_3\beta_3\gamma_{2S}$ $GABA_A$ receptors

Angelo Keramidas and Neil L. Harrison

Department of Anesthesiology and Department of Pharmacology, Columbia University, New York, NY 10032

The $\alpha_1\beta_2\gamma_2$ and $\alpha_3\beta_3\gamma_2$ are two isoforms of γ-aminobutyric acid type A ($GABA_A$) receptor that are widely distributed in the brain. Both are found at synapses, for example in the thalamus, where they mediate distinctly different inhibitory postsynaptic current profiles, particularly with respect to decay time. The two isoforms were expressed in HEK293 cells, and single-channel activity was recorded from outside-out patches. The kinetic characteristics of both isoforms were investigated by analyzing single-channel currents over a wide range of GABA concentrations. $\alpha_1\beta_2\gamma_2$ channels exhibited briefer active periods than $\alpha_3\beta_3\gamma_2$ channels over the entire range of agonist concentrations and had lower intraburst open probabilities at subsaturating concentrations. Activation mechanisms were constructed by fitting postulated schemes to data recorded at saturating and subsaturating GABA concentrations simultaneously. Reaction mechanisms were ranked according to log-likelihood values and how accurately they simulated ensemble currents. The highest ranked mechanism for both channels consisted of two sequential binding steps, followed by three conducting and three nonconducting configurations. The equilibrium dissociation constant for GABA at $\alpha_3\beta_3\gamma_2$ channels was ∼2.6 μM compared with ∼19 μM for $\alpha_1\beta_2\gamma_2$ channels, suggesting that GABA binds to the $\alpha_3\beta_3\gamma_2$ channels with higher affinity. A notable feature of the mechanism was that two consecutive doubly liganded shut states preceded all three open configurations. The lifetime of the third shut state was briefer for the $\alpha_3\beta_3\gamma_2$ channels. The longer active periods, higher affinity, and preference for conducting states are consistent with the slower decay of inhibitory currents at synapses that contain $\alpha_3\beta_3\gamma_2$ channels. The reaction mechanism we describe here may also be appropriate for the analysis of other types of $GABA_A$ receptors and provides a framework for rational investigation of the kinetic effects of a variety of therapeutic agents that activate or modulate $GABA_A$ receptors and hence influence synaptic and extrasynaptic inhibition in the central nervous system.

INTRODUCTION

γ-aminobutyric acid type A ($GABA_A$) receptors are a group of closely related yet biophysically and pharmacologically diverse receptors that belong to a larger family of ligand-activated ion channel receptors. All $GABA_A$ receptors are comprised of pentameric combinations of homologous subunits, and all subunits are members of a large gene family. In eukaryotes, members of this family are characterized by a functionally important loop in the extracellular domain of each subunit ("cys-loop") formed by a cysteine–cysteine bond. $GABA_A$ receptors are found in nature as distinct assemblies from a total of 16 known subunits (19 if you include the ρ subunits; Olsen and Sieghart, 2008). The functional role of $GABA_A$ receptors depends on their location, which itself depends to a large extent on subunit composition. Synaptic $GABA_A$ receptors mediate phasic inhibition and play a role in timing and synchronization, and these require a γ subunit to be trafficked to the synapse. In contrast, the δ subunit has been found only in extrasynaptic receptors. These $GABA_A$ receptors are tonically activated by ambient GABA in the perisynaptic space and are presumed to contribute to the control of basal excitability level (Mody and Pearce, 2004; Farrant and Nusser, 2005).

The most abundant and widely distributed synaptic $GABA_A$ receptor contains α_1, β_2, and γ_2 subunits at a ratio of 2:2:1 ($2\alpha_1 2\beta_2 1\gamma_2$). Another synaptic $GABA_A$ receptor, which is less abundant, is comprised of α_3, β_3, and γ_2 subunits. These two $GABA_A$ receptor subtypes are often located in the same neuroanatomical regions, such as the cortex and thalamus, but are confined to different nuclei, tissue layers, or cell types (Sieghart and Sperk, 2002). For instance, in the thalamus, the $GABA_A$ receptor found at the inhibitory synapses on thalamocortical neurons in the ventrobasal nucleus (VB) is the $\alpha_1\beta_2\gamma_2$ isoform, whereas the $GABA_A$ receptor found at the reciprocal inhibitory synapses between neurons in the reticular nucleus (RTN) is of the $\alpha_3\beta_3\gamma_2$ subtype. These two receptors have been carefully studied in expression systems and in brain slice preparations, where it has been reported that inhibitory postsynaptic currents (IPSCs) recorded from RTN decay much more slowly than IPSCs recorded from VB (Mozrzymas et al., 2007; Schofield and Huguenard, 2007; Jia et al., 2009). This

Correspondence to Angelo Keramidas: ak2963@columbia.edu

Abbreviations used in this paper: $GABA_A$, γ-aminobutyric acid type A; IPSC, inhibitory postsynaptic current; LL, log-likelihood; nACh, nicotinic acetylcholine; RI, rectification index; RTN, reticular nucleus; VB, ventrobasal nucleus.

The Rockefeller University Press $30.00
J. Gen. Physiol. Vol. 135 No. 1 59–75
www.jgp.org/cgi/doi/10.1085/jgp.200910317

observation strongly suggests that subunit composition is a possible determinant of the time course of synaptic currents, which in turn implies that subunit composition confers distinct kinetic properties on individual channels.

A considerable body of literature is now available on the relationship between structure and function of ligand-gated ion channels at the molecular level. The most thoroughly examined and understood of these channels are those belonging to the cys-loop family, and of these, the muscle nicotinic acetylcholine (nACh) receptor has been investigated most assiduously. One especially productive approach to investigating ion channels is to record single-channel currents, postulate reaction schemes for channel activation, and fit those schemes to the idealized data by maximum likelihood methods (Colquhoun and Hawkes, 1995; Qin et al., 1996; Colquhoun et al., 2003). Using this methodology, single-channel studies have yielded fine-grained structural information concerning interacting domains (Lee et al., 2009) and detected concerted microdomain movements involved in the transduction of agonist binding to channel opening (Grosman et al., 2000; Auerbach, 2005; Purohit et al., 2007). Similar studies that are compatible with the notion of discrete movements along the reaction pathway have revealed previously undiscovered functional states in the context of refined gating schemes that describe channel activation in both nACh and glycine receptors (Burzomato et al., 2004; Lape et al., 2008; Mukhtasimova et al., 2009).

Even though $GABA_A$ receptors are the main mediators of neuronal inhibition in the brain, fewer attempts have been made to apply a rigorous analytical treatment, with the notable exception of a study on $\alpha_1\beta_1\gamma_{2S}$ $GABA_A$ receptors (Lema and Auerbach, 2006). Several gating mechanisms have been proposed for $GABA_A$ receptor activation, and these describe the properties of ensemble (Jones and Westbrook, 1995) and single-channel (Steinbach and Akk, 2001) currents well, but a universally accepted mechanism that can be broadly applied to $GABA_A$ receptors is unavailable. Such a mechanism would be of use in describing and reconciling a broad spectrum of data on a variety of drugs that interact with $GABA_A$ receptors—from agonists, including "partial agonism" as recently elucidated for nACh and glycine receptors (Lape et al., 2008), to channel modulation by agents such as benzodiazepines and neurosteroids, and activation by anaesthetics (Krasowski and Harrison, 1999).

Here, we have developed and evaluated several reaction schemes that describe $GABA_A$ receptor activation, one of which we began to describe in a previous study (Keramidas and Harrison, 2008). The evaluation of these kinetic schemes was done initially on the basis of the log-likelihood (LL) values, which indicate the accuracy with which a postulated scheme fits single-channel records. The general applicability of the schemes was tested by fitting them to single-channel data obtained from two isoforms of $GABA_A$ receptor, the $\alpha_1\beta_2\gamma_{2S}$ and $\alpha_3\beta_3\gamma_{2S}$ channels. The best of these schemes were then used to simulate multichannel currents, and these simulations were compared with real macropatch currents in response to single and paired 1-ms pulses of agonist, providing an additional means of distinguishing schemes.

The mechanism that best satisfied our selection criteria consists of two sequential binding steps for GABA, leading to three shut and three open states and is similar in some ways to a mechanism proposed for $\alpha_1\beta_1\gamma_{2S}$ $GABA_A$ receptors (Lema and Auerbach, 2006). The best two mechanisms evaluated both involve a fully liganded shut channel transitioning to a second fully liganded shut state before entering any conducting configurations. The existence of preconducting states has recently been described in other cys-loop receptors (Burzomato et al., 2004; Lape et al., 2008; Mukhtasimova et al., 2009) and may be a common feature of the activation mechanism for the entire receptor family.

MATERIALS AND METHODS

Expression of $GABA_A$Rs in HEK293 cells

HEK293 cells were seeded onto poly-D-lysine–coated glass coverslips and transfected with cDNA encoding the human α_1, β_2, and γ_{2S} or α_3, β_3, and γ_{2S} subunits at a plasmid ratio of 1:1:4 (α:β:γ) using the calcium phosphate coprecipitation method. The cells were cotransfected with the CD4 surface antigen, which acted as a transfection marker. Transfected cells were washed after 24 h of exposure to the cDNA precipitate and used for patch clamp recordings 48–72 h later.

Electrophysiology and solutions

GABA-gated currents were recorded at room temperature (21 ± 1°C) using the excised outside-out patch configuration of the patch clamp technique. All patches were voltage clamped at a potential of −70 mV. Single-channel and macropatch currents were recorded using an Axopatch 200B amplifier (Axon Instruments), filtered with a four-pole Bessel filter that is built into the amplifier at a −3-dB value of 5 or 10 kHz, and acquired at a sampling frequency of 20 kHz (macropatch recordings) or 50 kHz (single-channel recordings). The standard extracellular solution contained (in mM): 140 NaCl, 5 KCl, 2 $CaCl_2$, 1 $MgCl_2$, 10 D-glucose, and 10 HEPES, and titrated to a pH of 7.4 with NaOH. The standard intracellular solution contained (in mM): 80 NaCl, 60 CsCl, 3 KCl, 2 K_2ATP, 4 $MgCl_2$, 1 $CaCl_2$, 5 EGTA, 10 D-glucose, and 10 HEPES, with pH adjusted to 7.4 with NaOH. Patch pipettes were made of standard wall borosilicate glass and had resistances of 6–15 MΩ when filled with intracellular solution. Pipettes used for single-channel recordings were also coated with a silicon polymer (Sylgard 184; Corning) and fire-polished to improve signal resolution. Single-channel (equilibrium) recordings were made in the continuous presence of agonist, which was dissolved at the desired concentration in the extracellular solution. Macropatch (non-equilibrium) recordings were done by positioning the patches near the solution interface of a double lumen glass tube mounted on a piezo-electric translator. Currents were elicited by exposing the patches to 5 mM GABA for either 1 ms or a pair of 1-ms pulses separated by 24 ms.

Data analysis

Plots of agonist-dependent variables (cluster or burst length and intraburst open probability, P_O) were fitted to a modified Hill equation of the form:

$$Y = \frac{Y^{\max}[A]^n}{[A]^n + EC_{50}^n} + y_0, \quad (1)$$

where *[A]* is the agonist concentration, EC_{50} is the concentration of agonist that produces half of the maximal response, n is the Hill coefficient (slope at EC_{50}), Y is the response to *[A]*, Y^{max} is the maximal response, and y_O is the lower limit of the response as *[A]* approaches 0.

Single-channel current amplitude was determined by generating amplitude histograms for selected segments of record and fitting the histograms to Gaussian curves. Single-channel conductance was calculated using the following expression:

$$\gamma = \frac{i}{(V_m - V_{rev})}, \quad (2)$$

where γ is the single-channel conductance, i is the single-channel current amplitude, V_m is the transmembrane potential, and V_{rev} is the potential at which current reverses direction (reversal potential). The values of V_{rev} were obtained from i-V measurements, covering a range of voltages between −70 and +70 mV. Liquid junction potential offsets were accounted for (using ion activities) in the conductance calculation. In addition, an estimate of current rectification (rectification index [RI]) over the experimental voltage range was determined by taking the ratio of current amplitude at −60 and +60 mV.

The activation rate (10–90% rise time) for macropatch currents was determined by fitting the following equation to middle 80% of the onset phase of currents.

$$I(t) = I_{\max}\left(1 - e^{-t/\tau}\right), \quad (3)$$

where *I(t)* is the current at time t, I_{max} is the maximum current, and τ is the time constant. The deactivation phase of macropatch currents was fitted with two standard exponential equations.

Single-channel kinetic analysis and modeling were done using QuB software (http://www.qub.buffalo.edu). A saturating concentration of 5 mM of agonist was initially used to isolate the gating steps from agonist binding. At this concentration, agonist binding preequilibrates, and the resulting activity arises from fully liganded channels. Periods of continuous activity were selected initially by eye and extracted to separate files within QuB for further analysis. These eye-selected segments were discrete and separated from each other by quiescent periods lasting at least 100 ms. Isolated brief openings that sometimes occurred between clusters and multiple openings within active periods were excluded during cluster selection and not included in any analysis (Fig. 3). The segmented *k*-means algorithm was used for idealizing the data, and the first and last shutting events of discrete active periods were dropped from the idealized data. The segments were then divided into clusters of activity by applying a critical shut time (t_{crit}) that marked the end of a cluster (Colquhoun and Hawkes, 1995). t_{crit} values were determined for each patch by generating shut-time dwell histograms of the idealized eye-selected segments of data. Some eye-selected segments produced several t_{crit} values, and the longest one (between the two longest components) was chosen and used to divide the eye-selected segments. This retained only three shut components in the distributions. For consistency, eye-selected segments that produced more shut components (as was the case with some selections in Fig. 3) with the initial fit were divided by a t_{crit} that retained the shortest three components. These preliminary fits were needed solely to determine t_{crit} values for the purpose of dividing eye-selected segments into shorter clusters of activity and were not used for further analysis. The t_{crit} values at 5 mM GABA ranged between 8–20 ms for the $\alpha_1\beta_2\gamma_{2S}$ $GABA_A$ receptors and 9–25 ms for the $\alpha_3\beta_3\gamma_{2S}$ $GABA_A$ receptors. The system dead time was 40 µs. The resulting clusters were analyzed for mean duration, open probability (intraburst P_O), and open and shut durations. The number of individual exponential components in each dwell class (shut or open) resulting from the final fit was taken as the minimum number of states in any underlying reaction scheme.

Subsaturating concentrations of GABA (200, 20, and 2 µM) were used to obtain information for agonist binding steps and were analyzed in the same way as the data obtained at 5 mM GABA. 200 µM GABA also produced clusters of activity at both channel isoforms. The t_{crit} values were chosen by the same methods as described for the 5-mM activity. At this concentration, the t_{crit} values were 19–31 ms for the $\alpha_1\beta_2\gamma_{2S}$ channels and 11–30 ms for the $\alpha_3\beta_3\gamma_{2S}$ channels. At 20 and 2 µM GABA, channel activity occurred as shorter, scattered bursts, and it was generally more difficult to isolate segments of activity that appeared to arise from a single channel, especially for the $\alpha_1\beta_2\gamma_{2S}$ isoform. In this case, we selected segments lasting several seconds that did not contain any overlapping openings and constructed shut histograms for these. A t_{crit} of 35 ms applied to this activity retained the three fastest components and a fourth that accounted for the binding steps for GABA. We also used a t_{crit} of 100 ms, retrospectively, to some 2 µM of data to determine if our original choice of 35 ms inadvertently excised some longer components associated with ligand binding.

Global fitting of data across concentrations was done by postulating a scheme that contained the number of fully liganded states (gating states) determined from the analysis of data at 5 mM GABA and adding two sequential binding steps to each of the doubly liganded shut states for evaluation. Schemes were fitted simultaneously to sets of data, with each set including data recorded at 5 mM, 200 µM, and 20 µM for $\alpha_1\beta_2\gamma_{2S}$ channels and 5 mM, 200 µM, and 2 µM for $\alpha_3\beta_3\gamma_{2S}$ channels. Data recorded at 2 µM for the $\alpha_1\beta_2\gamma_{2S}$ channels were not included in the initial global fitting analysis because this concentration induced mostly very short, sparse activity with too few complex bursts. However, the two patches that did yield sufficient complex activity were analyzed separately, included in separate datasets, and analyzed as described above to verify the agonist dissociation constant obtained from the initial global fitting.

Generating dwell histograms and fitting idealized data to schemes were done by the method of maximum likelihood. The dwell histograms were fitted with mixtures of probability density functions (Colquhoun and Hawkes, 1995; Lema and Auerbach, 2006). Each set of data produced a LL value, and the sums of LL values (ΣLL) were compared across all postulated schemes.

Single-channel currents in the presence of high concentrations of GABA often exhibit modal activity based on intraburst P_O (Lema and Auerbach, 2006; Keramidas and Harrison, 2008). In $\alpha_1\beta_2\gamma_{2S}$ $GABA_A$ receptors, the two prevalent gating modes are characterized by P_Os of ∼0.7 and ∼0.9. Both of these modes were evident in $\alpha_1\beta_2\gamma_{2S}$ and $\alpha_3\beta_3\gamma_{2S}$ single-channel records but were not treated separately in the analysis (Fig. 3). P_O values stated in the text represent the mean of high- and mid-P_O activity.

The derived schemes along with the mean rate constants from the single-channel analysis were used to generate simulations of macropatch currents in response to a single or a pair of 1-ms applications of agonist. These simulations were also done in QuB with the number of channels contributing to the currents set to 1,000. The simulated single-pulse currents were then analyzed for activation rate (10–90% rise time) and deactivation by fitting

single- or double-exponential equations, respectively, to the currents as described above for the real currents. For the paired-pulse simulations, the percentage change in the second peak relative to the first was measured and compared with that of the real paired-pulse currents for the $\alpha_1\beta_2\gamma_{2S}$ channels that we recorded or the $\alpha_3\beta_3\gamma_{2S}$ channels, which we obtained from the literature. Deactivation time constants for single-pulse responses of the $\alpha_3\beta_3\gamma_{2S}$ channels were also obtained from the literature.

Four of the schemes that were tested against the data (among others) are the following:

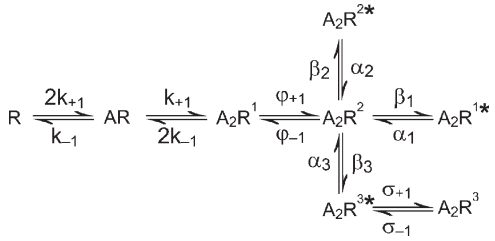

(SCHEME 1)

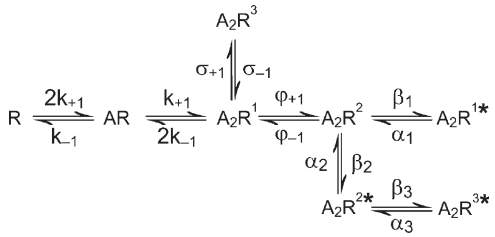

(SCHEME 2)

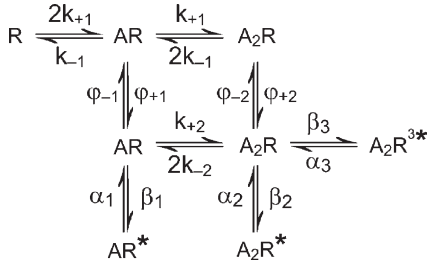

(SCHEME 3)

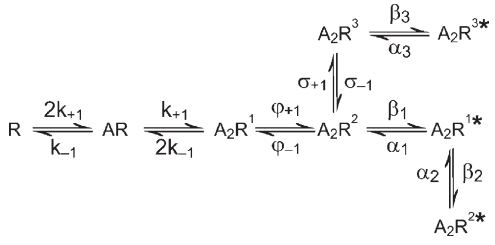

(SCHEME 4)

R represents the receptor, A represents the agonist, and AR and A_2R are the mono- and diliganded receptor in the closed state, respectively. The state number is denoted by a superscript on the right of the state, and an asterisk denotes an open, conducting channel. The symbols on either side of the double arrows are the microscopic rate constants governing the transitions to and from each state.

Scheme 1 is based on a gating scheme that was derived for $\alpha_1\beta_2\gamma_{2S}$ $GABA_A$ receptors expressed in outside-out patches in response to 10 mM GABA (Keramidas and Harrison, 2008). Scheme 2 was the highest ranking scheme obtained from comparable analysis of $\alpha_1\beta_1\gamma_{2S}$ $GABA_A$ receptors also expressed in HEK293 cells, but in the cell-attached configuration (Lema and Auerbach, 2006), and Scheme 3 is based on a mechanism that was derived from single-channel analysis of the muscle-type nACh receptor (Lape et al., 2008). Microscopic reversibility was applied to the loop part of Scheme 3. Scheme 4 was one of the top-ranking schemes in terms of LL values and the simulation of macropatch currents. In total, 20 distinct schemes were tested. Data are stated as mean ± SEM for (n) separate experiments (recorded patches or datasets).

RESULTS

Single-channel activity and amplitude

Single-channel currents were initially recorded from excised outside-out membrane patches expressing either $\alpha_1\beta_2\gamma_{2S}$ or $\alpha_3\beta_3\gamma_{2S}$ $GABA_A$ receptors in the presence of 5 mM GABA. Both $\alpha_1\beta_2\gamma_{2S}$ and $\alpha_3\beta_3\gamma_{2S}$ $GABA_A$ receptors exhibited visibly similar single-channel activity, examples of which are shown in Fig. 1. Active periods occurred as discrete clusters of openings and shuttings, separated by quiescent periods lasting from generally ~15 ms to several minutes (see also Fig. 3). Two current amplitudes were evident in most patches. The predominant level was just under −2 pA at a holding potential of −70 mV (Fig. 1, A and C, bottom record), but the channels also opened to a smaller level of about −1.2 pA. For both channel types, the smaller amplitude occurred either as brief transitions from the larger amplitude openings, as shown in Fig. 1 A for $\alpha_1\beta_2\gamma_{2S}$ $GABA_A$ receptors, or as separate active periods, as illustrated by the cluster of activity in Fig. 1 C (top record) for $\alpha_3\beta_3\gamma_{2S}$ $GABA_A$ receptors.

To obtain estimates of single-channel amplitudes at −70 mV, amplitude histograms were plotted and fitted with Gaussian curves for both channel types. Examples of these plots are shown in Fig. 1 (B and D) for the accompanying recordings. For $\alpha_1\beta_2\gamma_{2S}$ $GABA_A$ receptors, the mean amplitude of the most prevalent openings was −1.81 ± 0.05 pA (n = 7), whereas the smaller, rarer activity was −1.11 ± 0.04 pA (n = 6). For the $\alpha_3\beta_3\gamma_{2S}$ $GABA_A$ receptors, the more common, larger openings had a mean amplitude of −1.66 ± 0.03 pA (n = 5) and the smaller currents were −1.02 ± 0.05 pA (n = 8). The measurements for the larger openings are similar to previously published values for $\alpha_1\beta_2\gamma_{2S}$ $GABA_A$ receptors (Keramidas and Harrison, 2008) and $\alpha_3\beta_2\gamma_{2S}$ $GABA_A$ receptors (Barberis et al., 2007). It should be noted that the smaller openings are not likely mediated by binary αβ channels, as these do not exhibit long clusters of activity (Wagner et al., 2004) nor are they likely

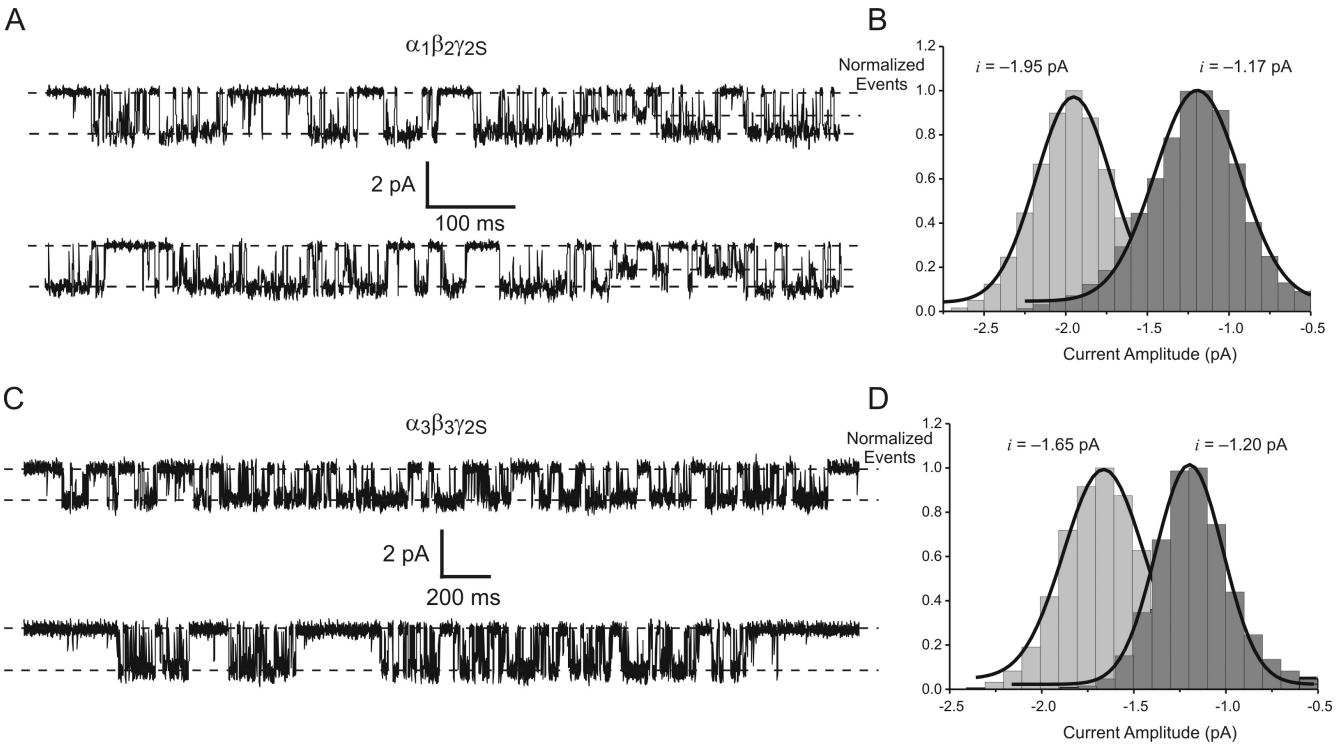

Figure 1. Conductance levels of $\alpha_1\beta_2\gamma_{2S}$ and $\alpha_3\beta_3\gamma_{2S}$ $GABA_A$ receptors. (A) Continuous sweeps of single-channel activity recorded from a patch expressing $\alpha_1\beta_2\gamma_{2S}$ $GABA_A$ receptors in the presence of 5 mM GABA. Note the two conductance levels indicated by broken lines and the transition from the larger conductance to the smaller, and back again. (B) Amplitude histograms for the data shown in A. The two amplitudes are indicated on the plot. (C) Two separate segments of single-channel activity recorded from the same patch expressing $\alpha_3\beta_3\gamma_{2S}$ $GABA_A$ receptors in the presence of 5 mM GABA. The two conductance levels can also occur as discrete long clusters of either the small conductance (top trace) or the large conductance (bottom trace). (D) Amplitude histograms for the data shown in C. The two amplitudes are indicated on the plot. Openings are downward deflections, and the holding potential was −70 mV in both cases.

to appear as transitions within clusters of the larger amplitude activity.

Current–voltage relationships

For the purpose of obtaining estimates of single-channel conductance and investigating current rectification, single-channel currents were recorded over a voltage range of −70 to +70 mV for each patch. The larger current amplitudes were plotted as a function of membrane potential for each channel type. The group plots, accompanied by an example of an experiment from a single patch, are shown for $\alpha_1\beta_2\gamma_{2S}$ $GABA_A$ receptors in Fig. 2 A and for $\alpha_3\beta_3\gamma_{2S}$ $GABA_A$ receptors in Fig. 2 B. From these plots, the reversal potential was read and the conductance for each channel was computed using Eq. 2, after correcting for liquid junction potentials. The reversal potential for $\alpha_1\beta_2\gamma_{2S}$ $GABA_A$ receptors was 0.9 ± 0.2 mV (n = 7) and for $\alpha_3\beta_3\gamma_{2S}$ $GABA_A$ receptors was 0.9 ± 0.3 mV (n = 5). The reversal potential of the smaller current amplitude was assumed to be the same as the corresponding larger amplitude for the same channel type. As can be seen in Fig. 2 and Table I, the main and lower conductance values of $\alpha_1\beta_2\gamma_{2S}$ $GABA_A$ receptors were 24.5 ± 0.7 pS (n = 7) and 15.1 ± 0.5 pS (n = 6), respectively, and for $\alpha_3\beta_3\gamma_{2S}$ $GABA_A$ receptors were 22.7 ± 0.5 pS (n = 5) and 14.3 ± 0.7 pS (n = 8), respectively. There was also little evidence of current rectification in either channel, with the RI for $\alpha_1\beta_2\gamma_{2S}$ channels being 1.21 ± 0.02 (n = 7) and that for $\alpha_3\beta_3\gamma_{2S}$ channels being 1.15 ± 0.03 (n = 5; Table I).

Discrete segments of activity of the low conductance type, as is shown for the $\alpha_3\beta_3\gamma_{2S}$ channels in the top trace of Fig. 1 C and for $\alpha_1\beta_2\gamma_{2S}$ channels in Fig. 3 A (e), were quite rare. Out of 18 patches expressing $\alpha_1\beta_2\gamma_{2S}$ channels at 5 mM or 200 μM GABA, only four exhibited low conductance clusters that were >1-s long (a combined total of ∼1,000 events). The $\alpha_3\beta_3\gamma_{2S}$ channels showed a similar reluctance to activate to the low conductance openings. From 33 patches at the higher GABA concentrations, only five low conductance clusters longer than 1 s were observed (a combined total of ∼1,500 events).

TABLE I

Single-channel conductance and rectification of $\alpha_1\beta_2\gamma_{2S}$ and $\alpha_3\beta_3\gamma_{2S}$ $GABA_A$ receptors

γ at −70 mV	γ1 (main, pS)	γ2 (pS)	RI (i–60 mV/i+60 mV)
$\alpha_1\beta_2\gamma_{2S}$	24.5 ± 0.7 (n = 7)	15.1 ± 0.5 (n = 6)	1.21 ± 0.02 (n = 7)
$\alpha_3\beta_3\gamma_{2S}$	22.7 ± 0.5 (n = 5)	14.3 ± 0.7 (n = 8)	1.15 ± 0.03 (n = 5)

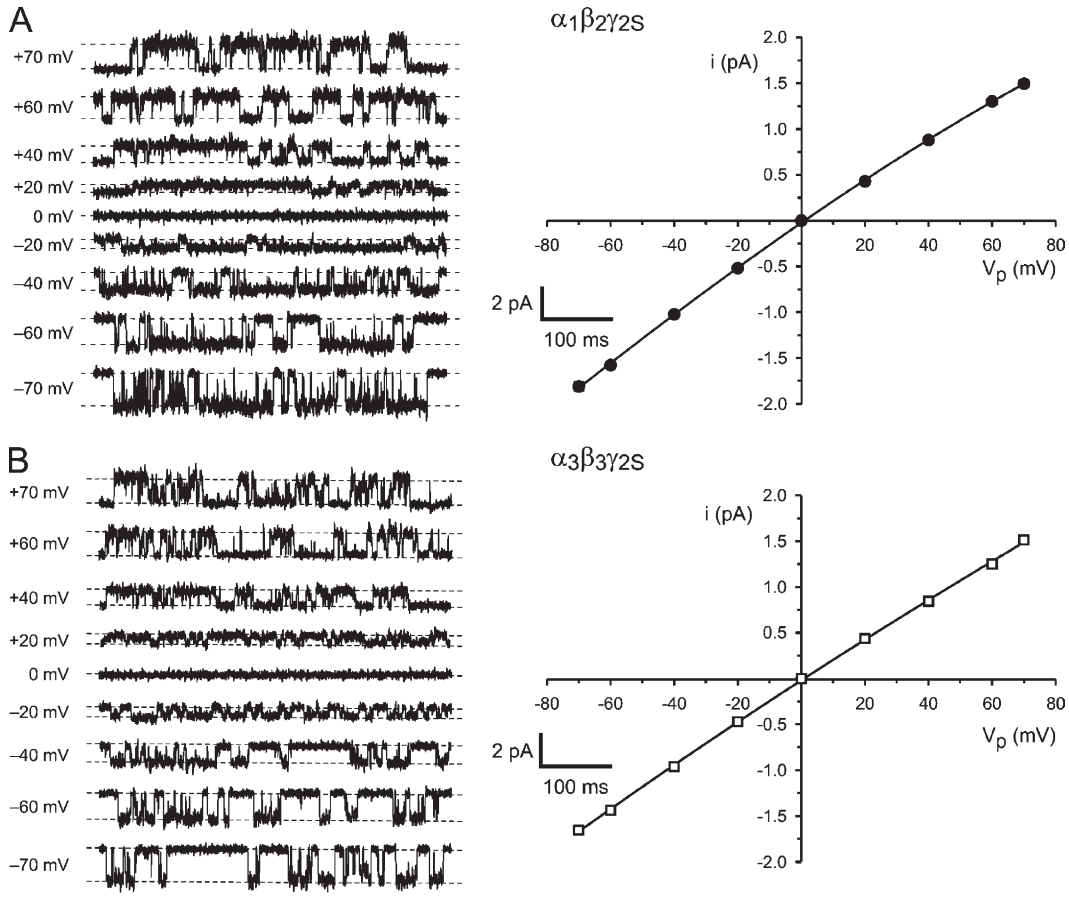

Figure 2. Current–voltage experiments for $\alpha_1\beta_2\gamma_{2S}$ and $\alpha_3\beta_3\gamma_{2S}$ $GABA_A$ receptors. (A) Single-channel activity recorded from the same patch expressing $\alpha_1\beta_2\gamma_{2S}$ $GABA_A$ receptors in the presence of 5 mM GABA. (B) Single-channel activity recorded from the same patch expressing $\alpha_3\beta_3\gamma_{2S}$ $GABA_A$ receptors in the presence of 5 mM GABA. The holding potential for each segment of record is indicated on the far left. On the right of each family of traces are the corresponding group plots of single-channel current amplitude (only the larger conductance openings are potted) as a function of holding potential. The group plots represent data from seven patches for the $\alpha_1\beta_2\gamma_{2S}$ channels and five patches for $\alpha_3\beta_3\gamma_{2S}$ channels. Note the very slight downward concavity of the i-V plots indicating mild inward rectification.

The remainder of patches for both channel isoforms exhibited much shorter (~10–50 ms), sporadic periods of low conductance activity that were discrete. Low conductance openings that occurred as brief transitions from the high to the low conductance, as illustrated in Fig. 1 A, were more frequently seen but also very short lived. Due to the paucity of low conductance data, we decided to analyze further only the high conductance currents. In our attempts to derive activation mechanisms, we were careful to reject low conductance periods that were either discrete or constituted more than ~2–3% of the overall length the high conductance active periods by scanning the records at high resolution.

Burst length and intraburst open probability

The next set of experiments was aimed at characterizing the kinetic differences between $\alpha_1\beta_2\gamma_{2S}$ and $\alpha_3\beta_3\gamma_{2S}$ $GABA_A$ receptors. To this end, single-channel currents were recorded over a wide range of GABA concentrations, and the duration and intraburst open probabilities were measured and plotted as a function of GABA concentration. For $\alpha_1\beta_2\gamma_{2S}$ $GABA_A$ receptors, the agonist concentrations used were 5 mM, 200 μM, 20 μM, and 2 μM, whereas 5 mM, 200 μM, and 2 μM GABA were used for $\alpha_3\beta_3\gamma_{2S}$ $GABA_A$ receptors.

Discrete segments of data lasting from hundreds of milliseconds to several seconds were selected (Fig. 3) for subdivision into active periods (clusters or bursts). These were determined by applying a critical shut time (t_{crit}), which separated one active period from the next (Colquhoun and Hawkes, 1995). A t_{crit} was determined for each patch and generally ranged between 8 and 35 ms for both channel types at the concentrations tested, although the mean t_{crit} values at 5 mM GABA were a little lower, being ~10 and ~12 ms for the $\alpha_1\beta_2\gamma_{2S}$ and $\alpha_3\beta_3\gamma_{2S}$ channels, respectively. With decreasing GABA concentrations, there was a corresponding decrease in cluster length and intraburst P_O.

Although cluster length decreased with decreasing GABA concentration, the clusters exhibited by $\alpha_3\beta_3\gamma_{2S}$

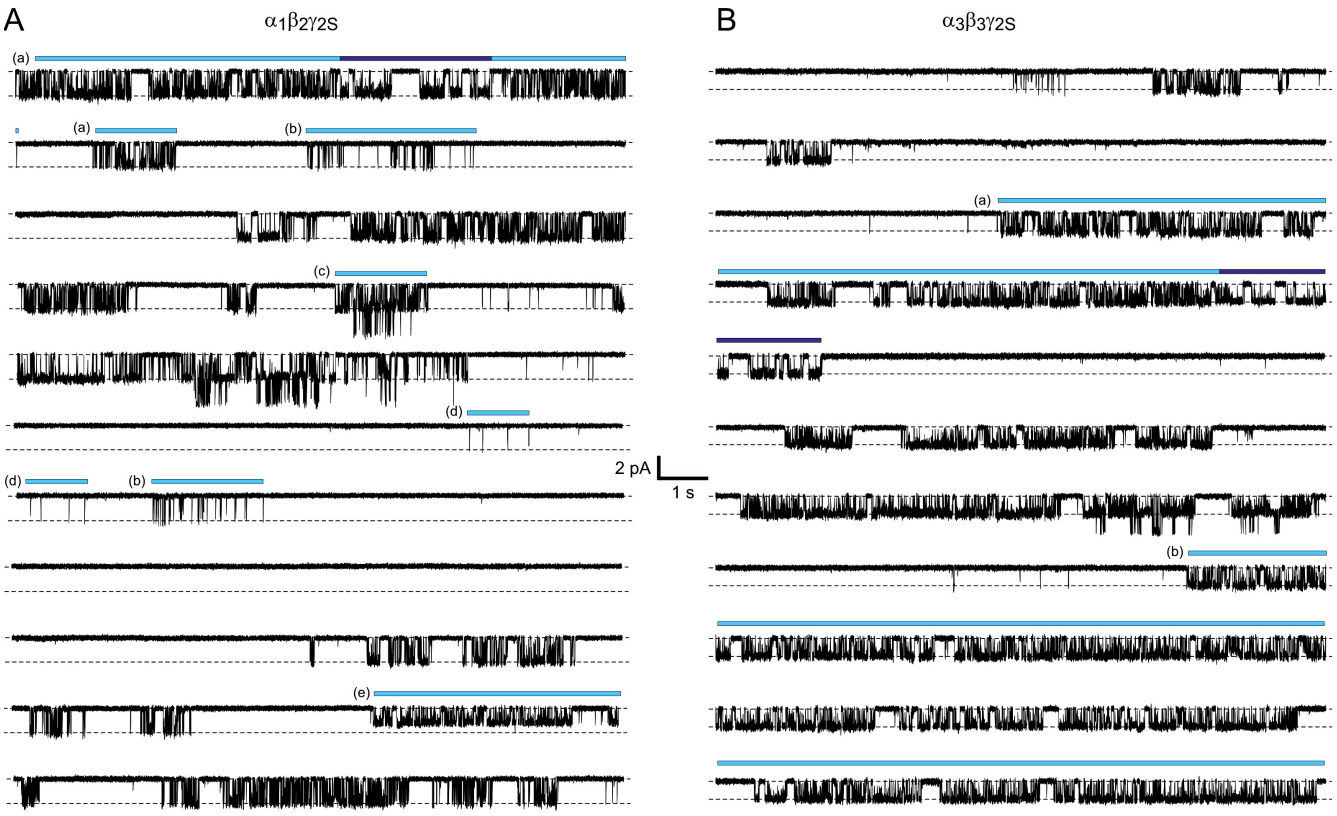

Figure 3. Selecting segments for kinetic analysis. (A) A low-time resolution recording from a patch expressing $\alpha_1\beta_2\gamma_{2S}$ $GABA_A$ receptors in response to 5 mM GABA. Stretches of single-channel activity were selected by eye and subsequently divided into discrete clusters by applying a critical shut time (t_{crit}). The most common type of activity (a) was of a high conductance and included segments with an intermediate and high (purple) intra-cluster P_O. Segments were excluded if they exhibited low P_O (b), had inconsistent single-channel conductance, contained overlapping activity from multiple channels (c), occurred as isolated openings (d), or were mainly of the low single-channel conductance (e). (B) A low-time resolution recording from a patch expressing $\alpha_3\beta_3\gamma_{2S}$ $GABA_A$ receptors in response to 5 mM GABA. Segments of activity (a) that were selected by eye include intermediate and high (purple) intra-cluster P_O. $\alpha_3\beta_3\gamma_{2S}$ $GABA_A$ receptors generally activated for longer continuous periods (b) compared with $\alpha_1\beta_2\gamma_{2S}$ $GABA_A$ receptors. Records were filtered to 1.5 kHz for display.

$GABA_A$ receptors were consistently longer than those of $\alpha_1\beta_2\gamma_{2S}$ $GABA_A$ receptors at the same concentration, as shown in Fig. 4 A. Exposing the $\alpha_1\beta_2\gamma_{2S}$ channels to 5 mM GABA elicited clusters that were 114 ± 11–ms (n = 7) long, which is similar to previously published measurements (Keramidas and Harrison, 2008). In contrast, 5 mM GABA elicited substantially longer clusters at $\alpha_3\beta_3\gamma_{2S}$ channels, being 196 ± 16 ms (n = 16). The mean cluster length in response to 200 µM GABA of $\alpha_1\beta_2\gamma_{2S}$ $GABA_A$ receptors was 83.5 ± 13.3 ms (n = 11) and for $\alpha_3\beta_3\gamma_{2S}$ $GABA_A$ receptors was 162 ± 22 ms (n = 17). 20 µM GABA elicited 45.5 ± 5.0 ms (n = 4) bursts at $\alpha_1\beta_2\gamma_{2S}$ $GABA_A$ receptors, and 2 µM GABA elicited 17.8± 3.0 ms (n = 5) and 51.5 ± 2.6 ms (n = 9) bursts at $\alpha_1\beta_2\gamma_{2S}$ and $\alpha_3\beta_3\gamma_{2S}$ $GABA_A$ receptors, respectively (see also Figs. 5 and 6). Intraburst P_O was also greater at $\alpha_3\beta_3\gamma_{2S}$ $GABA_A$ receptors, but only for GABA concentrations below 5 mM (Fig. 4 B). For the $\alpha_1\beta_2\gamma_{2S}$ channels, the P_O values were: 0.81 ± 0.01 (n = 7; 5 mM GABA), 0.61 ± 0.04 (n = 11; 200 µM GABA), 0.33 ± 0.06 (n = 4; 20 µM GABA), and 0.15 ± 0.01 (n = 5; 2 µM GABA). For $\alpha_3\beta_3\gamma_{2S}$ channels, the P_O values were: 0.77 ± 0.02 (n = 16; 5 mM GABA), 0.69 ± 0.02 (n = 17; 200 µM GABA), and 0.45 ± 0.01 (n = 9; 2 µM GABA). Both channels exhibited modal gating with high-, mid-, and occasional low-P_O activity present in individual patches. At 5 mM GABA (n = 3 patches) and 200 µM GABA (n = 3 patches), the mid-mode activity was the most frequent and accounted for 80–90% of the activity for both channels. Modal switching was also evident when inspecting long segments of data (Fig. 3, purple). We excluded low-P_O clusters and conflated the high- and mid-P_O in our analysis.

Analysis of open and shut durations within active periods

The analysis of clusters and bursts of activity was extended to include measurements of dwell-time distributions across GABA concentrations for both channels. Fig. 5 shows typical recordings obtained from patches expressing $\alpha_1\beta_2\gamma_{2S}$ $GABA_A$ receptors. As mentioned above, as GABA concentration was lowered, active periods were abbreviated and the intraburst open probability also decreased. On the right of each record are

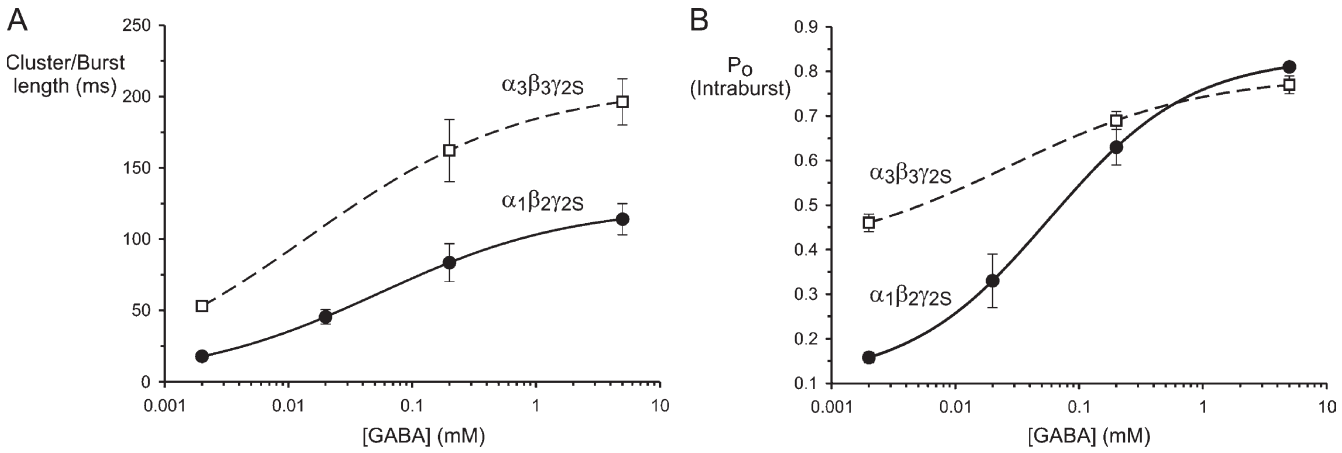

Figure 4. Burst length and intraburst P_O. (A) Plot of the cluster (5 mM and 200 µM GABA) or burst (20 and 2 µM GABA) durations as a function of GABA concentration for $\alpha_1\beta_2\gamma_{2S}$ $GABA_A$ receptors (filled circles) and $\alpha_3\beta_3\gamma_{2S}$ $GABA_A$ receptors (open squares). (B) Plot of intraburst P_O as a function of GABA concentration for $\alpha_1\beta_2\gamma_{2S}$ $GABA_A$ receptors (filled circles) and $\alpha_3\beta_3\gamma_{2S}$ $GABA_A$ receptors (open squares). The data for both plots were fitted to a Hill-type equation.

the open and shut dwell histograms for clusters (5 mM and 200 µM) and bursts (≤20 µM), which are fitted with mixtures of probability density functions. The time constants and fractions for each component are summarized in Table II. Three exponential components were required to adequately describe each dwell class (shut or open) at 5 mM and 200 µM GABA. Although the open time constants and fractions did not vary much between these two concentrations, the latter two shut-time constants increased with 200 µM GABA. Applying 20 µM GABA resulted in a further increase in the latter two shut-time constants and the introduction of a fourth, without any substantial change in the open component parameters (Table II and Fig. 5).

The $\alpha_3\beta_3\gamma_{2S}$ $GABA_A$ receptors were similarly analyzed. Fig. 6 shows examples of single-channel activity of $\alpha_3\beta_3\gamma_{2S}$ channels at 5 mM, 200 µM, and 2 µM GABA along with corresponding dwell histograms. Channel activity was also best described with three shut and three open components, with the first two shut components remaining little changed across concentrations. At 2 µM GABA, the third shut component increased and a fourth was also required to fit the histograms adequately. The second and third open components decreased with decreasing concentrations in contrast to those describing the $\alpha_1\beta_2\gamma_{2S}$ channels (Table III). The open and shut dwell-time constants for the $\alpha_3\beta_3\gamma_{2S}$ channels were generally higher than the corresponding values for the $\alpha_1\beta_2\gamma_{2S}$ channels.

Fitting single-channel data to postulated kinetic schemes

The dwell-time distribution analysis provided the basis for building kinetics schemes that describe the activation of $\alpha_1\beta_2\gamma_{2S}$ and $\alpha_3\beta_3\gamma_{2S}$ $GABA_A$ receptors by GABA. The number of components in the dwell-time distributions at saturating GABA concentrations (5 mM) was taken to represent the minimum number of diliganded states in the postulated kinetic schemes. Records obtained at subsaturating agonist concentrations, where the binding of agonist molecules becomes increasingly significant in the record with decreasing concentration, were exploited for obtaining information about agonist binding steps. Several schemes comprised of three shut and three open states were first tested for adequacy of fit to clusters of activity induced by 5 mM GABA. The states in each scheme were connected in various combinations and

TABLE II

Dwell time distributions for $\alpha_1\beta_2\gamma_{2S}$ $GABA_A$ receptors

	Shut				Open		
				5 mM GABA (n = 7)			
τ (ms)	0.172 ± 0.014	0.809 ± 0.102	3.13 ± 0.37	–	0.477 ± 0.024	2.64 ± 0.14	7.44 ± 0.65
Fraction	0.65 ± 0.03	0.18 ± 0.03	0.17 ± 0.03	–	0.18 ± 0.02	0.61 ± 0.07	0.21 ± 0.05
				200 µM GABA (n = 11)			
τ (ms)	0.216 ± 0.017	1.15 ± 0.09	5.9 ± 0.35	–	0.459 ± 0.063	2.75 ± 0.40	7.36 ± 0.88
Fraction	0.51 ± 0.04	0.17 ± 0.02	0.30 ± 0.03	–	0.23 ± 0.02	0.48 ± 0.04	0.28 ± 0.04
				20 µM GABA (n = 4)			
τ (ms)	0.390 ± 0.067	2.35 ± 0.46	10.4 ± 1.7	32.7 ± 5.0	0.469 ± 0.091	1.81 ± 0.45	5.66 ± 1.06
Fraction	0.38 ± 0.06	0.15 ± 0.03	0.18 ± 0.02	0.32 ± 0.32	0.53 ± 0.03	0.26 ± 0.08	0.21 ± 0.06

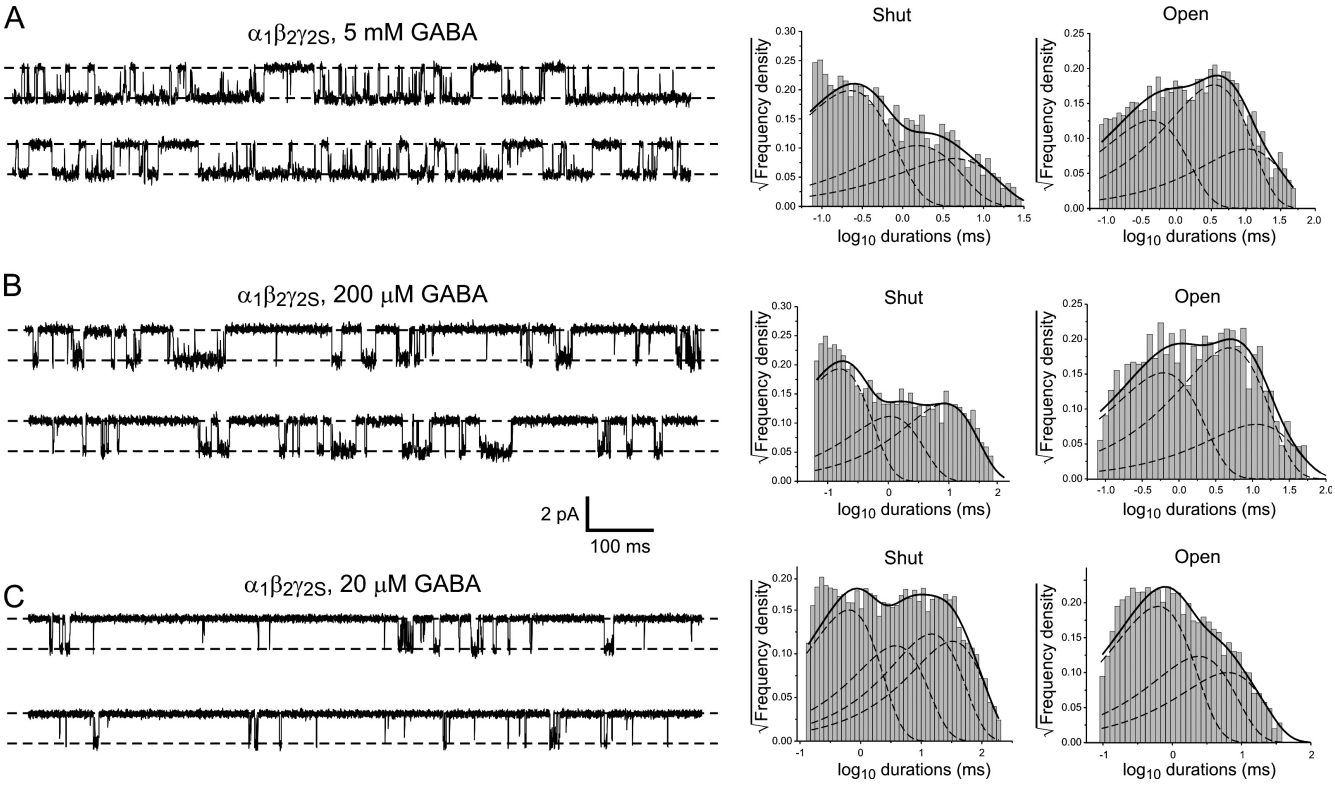

Figure 5. Single-channel activity across GABA concentrations for $\alpha_1\beta_2\gamma_{2S}$ $GABA_A$ receptors. Pairs of continuous sweeps of single-channel activity recorded from patches expressing $\alpha_1\beta_2\gamma_{2S}$ $GABA_A$ receptors in the presence of the GABA concentrations indicated. The records from A and B are from the same patch. On the right of each pair of traces are the corresponding dwell-time distributions for apparent shut and open times. The solid line fit represents a mixture of probability density functions, and the broken lines are the individual components.

tested for goodness of fit to five to seven patches expressing either $\alpha_1\beta_2\gamma_{2S}$ or $\alpha_3\beta_3\gamma_{2S}$ channels. Schemes were evaluated by summing the individual LL values for each dataset (for each channel type) and comparing the sum of LLs (ΣLL) from each scheme. We chose to focus on the best three of these schemes for further analysis. To these, we added a fourth (Scheme 3) for evaluation. To extend and reevaluate the schemes tested at 5 mM GABA, binding steps were included and fitted to data recorded at less than saturating GABA concentrations in conjunction with data obtained at 5 mM GABA. Each of the two binding steps was assumed to occur equivalently and independently. The binding steps were arranged in series and connected to either one of the three shut states (A_2R^1, A_2R^2, or A_2R^3) for global fitting. Mechanisms were fitted to four datasets, each set containing records at three GABA concentrations, for both channels. One 5-mM and one 20-μM record were used twice in the $\alpha_1\beta_2\gamma_{2S}$ channel analysis, and one 2-μM record was used twice for the $\alpha_3\beta_3\gamma_{2S}$ channel analysis. As before, LL values were used to rank schemes. These values are shown in Table IV for the best three schemes (Schemes 1, 2, and 4) and Scheme 3, which produced either low LL values or failed to successfully fit the data. In cases where Scheme 3 did not fit the datasets, the fitting algorithm failed to converge. For a single dataset of $\alpha_1\beta_2\gamma_{2S}$ channel activity, the fit was successful, and we tried to refit the other three datasets using the rate constants computed from that fit, but this also either failed (two cases) or produced an LL value that was <15,000, along with visibly poor fits of the corresponding dwell histograms (one case). For the $\alpha_3\beta_3\gamma_{2S}$ channels, all attempts to fit Scheme 3 resulted in nonconvergence of the fitting algorithm.

Table IV also shows the mean K_d values for each scheme. For the $\alpha_1\beta_2\gamma_{2S}$ receptors, Scheme 1 yielded higher LL values for three out of four datasets, and Scheme 4 was the leading scheme for the fourth dataset. Scheme 2 produced competitive LL values but always lagged behind Schemes 1 and 4. Overall, Scheme 1 produced the highest ΣLL, but it was only marginally higher than that for Scheme 4. There was a greater difference in the K_d values between schemes, with Scheme 1 producing the lowest K_d (highest affinity). The affinity values for the $\alpha_3\beta_3\gamma_{2S}$ receptors were very similar for Schemes 1, 2, and 4 and substantially lower than those for the $\alpha_1\beta_2\gamma_{2S}$ receptors. Again, Scheme 1 emerged with the highest ΣLL, closely followed by Scheme 4.

Our analysis on the basis of LL fitting suggests that Scheme 1 describes the data most accurately, with

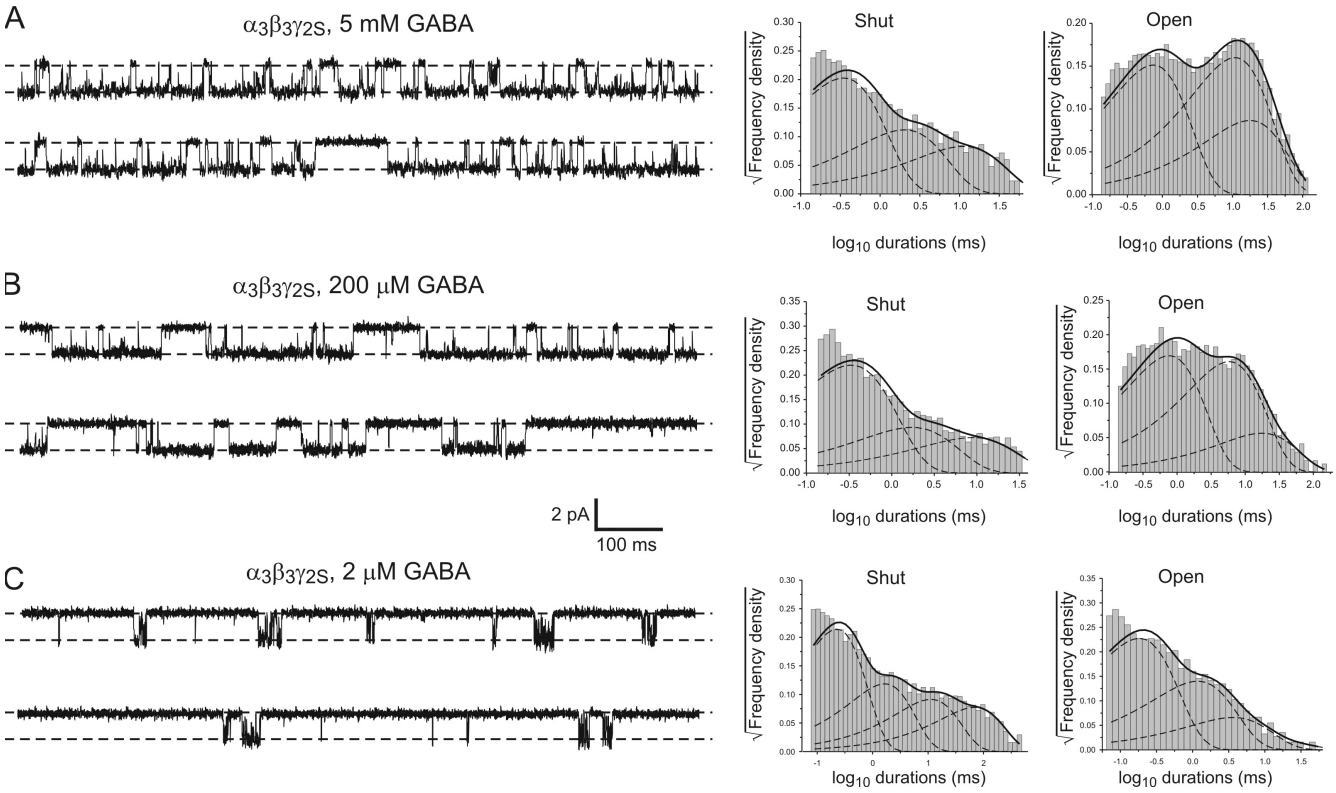

Figure 6. Single-channel activity across GABA concentrations for $\alpha_3\beta_3\gamma_{2S}$ $GABA_A$ receptors. Pairs of continuous sweeps of single-channel activity recorded from patches expressing $\alpha_3\beta_3\gamma_{2S}$ $GABA_A$ receptors in the presence of the GABA concentrations indicated. On the right of each pair of traces are the corresponding dwell-time distributions for apparent shut and open times. The solid line fit represents a mixture of probability density functions, and the broken lines are the individual components.

Scheme 4 being the nearest competitor. The global fitting yielded state transition rate constants for Scheme 1 for the $\alpha_1\beta_2\gamma_{2S}$ channels. These were: $k_{+1} = (17.0 \pm 3.6) \times 10^6\ M^{-1}s^{-1}$; $k_{-1} = 330 \pm 56\ s^{-1}$; $\phi_{+1} = 521 \pm 49\ s^{-1}$; $\phi_{-1} = 1{,}362 \pm 149\ s^{-1}$; $\beta_1 = 1{,}684 \pm 155\ s^{-1}$; $\alpha_1 = 340 \pm 67\ s^{-1}$; $\beta_2 = 1{,}660 \pm 357\ s^{-1}$; $\alpha_2 = 1{,}986 \pm 188\ s^{-1}$; $\beta_3 = 223 \pm 98\ s^{-1}$; $\alpha_3 = 205 \pm 42\ s^{-1}$; $\sigma_{+1} = 1{,}216 \pm 134\ s^{-1}$; and $\sigma_{-1} = 153 \pm 36\ s^{-1}$ ($n = 4$; Fig. 7 A). Similarly, for the $\alpha_3\beta_3\gamma_{2S}$ channels, the rate constants for Scheme 1 were: $k_{+1} = (51.0 \pm 0.6) \times 10^6\ M^{-1}s^{-1}$; $k_{-1} = 134 \pm 25\ s^{-1}$; $\phi_{+1} = 396 \pm 34\ s^{-1}$; $\phi_{-1} = 1{,}275 \pm 143\ s^{-1}$; $\beta_1 = 3{,}003 \pm 274\ s^{-1}$; $\alpha_1 = 895 \pm 228\ s^{-1}$; $\beta_2 = 742 \pm 28\ s^{-1}$; $\alpha_2 = 192 \pm 51\ s^{-1}$; $\beta_3 = 534 \pm 149\ s^{-1}$; $\alpha_3 = 645 \pm 55\ s^{-1}$; $\sigma_{+1} = 1{,}940 \pm 243\ s^{-1}$; and $\sigma_{-1} = 2{,}509 \pm 118\ s^{-1}$ ($n = 4$; Fig. 7 B).

To facilitate a comparison between key kinetic differences between $\alpha_1\beta_2\gamma_{2S}$ and $\alpha_3\beta_3\gamma_{2S}$ $GABA_A$ receptor activation, the equilibrium constants for the transition of each state was calculated and tabulated (Table V). Most equilibrium constants were either not distinguishable (Φ) or differed by only two- to fivefold (E_1, E_2, and E_3). The equilibrium constants that varied most between the two channels were the dissociation equilibrium

TABLE III

Dwell-time distributions for $\alpha_3\beta_3\gamma_{2S}$ $GABA_A$ receptors

	Shut				Open		
			5 mM GABA ($n = 16$)				
τ (ms)	0.303 ± 0.014	1.28 ± 0.08	5.21 ± 0.42	–	0.628 ± 0.031	4.11 ± 0.80	10.8 ± 1.5
Fraction	0.72 ± 0.03	0.15 ± 0.02	0.13 ± 0.02	–	0.44 ± 0.03	0.39 ± 0.04	0.17 ± 0.04
			200 μM GABA ($n = 17$)				
τ (ms)	0.255 ± 0.015	1.27 ± 0.18	5.51 ± 0.54	–	0.551 ± 0.038	2.80 ± 0.41	10.4 ± 0.17
Fraction	0.76 ± 0.06	0.18 ± 0.01	0.12 ± 0.02	–	0.43 ± 0.02	0.41 ± 0.02	0.17 ± 0.03
			2 μM GABA ($n = 7$)				
τ (ms)	0.318 ± 0.020	1.59 ± 0.12	11.5 ± 1.8	38.3 ± 4.4	0.644 ± 0.069	1.73 ± 0.21	4.26 ± 0.14
Fraction	0.64 ± 0.02	0.14 ± 0.02	0.11 ± 0.02	0.11 ± 0.02	0.42 ± 0.04	0.44 ± 0.03	0.66 ± 0.02

TABLE IV

LL values for Schemes 1, 2, 3, and 4

Channel	Data set	Total no. of transitions	LL per data set			
			S1	S2	S3	S4
$\alpha_1\beta_2\gamma_{2S}$	1	21,631	135,053	134,988	112,568	135,041
	2	21,360	117,694	116,626	NC	117,670
	3	24,273	134,715	133,501	NC	134.670
	4	20,460	124,399	124,099	NC	124,421
ΣLL			511,861	509,214	112,568	511,802
K_d (μM)			19.4	132	0.7	96.3
$\alpha_3\beta_3\gamma_{2S}$	1	43,097	231,236	220,014	NC	231,229
	2	31,145	170,226	168,407	NC	170,199
	3	24,405	135,771	134,984	NC	135,688
	4	25,460	136,387	134,549	NC	136,377
ΣLL			673,620	657,954	–	673,493
K_d (μM)			2.63	3.07	–	2.67

constant, K_d, and the transition constant, Σ. These were, respectively, over sevenfold and 10-fold higher for the $\alpha_1\beta_2\gamma_{2S}$ channels than for the $\alpha_1\beta_2\gamma_{2S}$ channels.

We did not include single-channel data from $\alpha_1\beta_2\gamma_{2S}$ $GABA_A$ receptors in the presence of 2 μM GABA in our main datasets for global fitting. This was because most records at this concentration did not produce sufficient bursts of activity, and it was generally difficult to confidently select segments of data that were generated by a single channel. At this concentration, however, binding steps would be even more prominent in the record than at 20 μM GABA and potentially provide the most information regarding K_d. Nevertheless, we endeavored to check our estimate of K_d for the $\alpha_1\beta_2\gamma_{2S}$ channels. Two relatively long-lasting patches at 2 μM GABA gave a sufficient number of short bursts of activity (total of ∼3,000 and ∼1,950 events), which were analyzed separately and in combination with data recorded at 20 and 200 μM GABA for global fitting. We first tested if our choice of t_{crit} affected the computed value of K_d. A t_{crit} of 35 ms applied to the 2-μM GABA data yielded the same K_ds as a t_{crit} of 100 ms for both patches, validating our original choice of t_{crit}. Second, we tested if K_d was dead-time sensitive with global fitting analysis. A dead time of 40 μs produced K_ds of 17.8 μM (dataset 1) and 29.2 μM (dataset 2). Increasing the dead time to 70 μs yielded K_ds of 17.4 and 30.6 μM, respectively, suggesting that the K_d estimates were not dead-time sensitive to an appreciable extent.

Macropatch current simulations

It has been suggested that nonequilibrium data can help discriminate between statistically similar mechanistic schemes that were derived using equilibrium data (Kienker, 1989). As an additional test for our schemes, we either measured salient kinetic parameters from macropatch currents we recorded or obtained them from the literature (Table VI). Currents were evoked in patches expressing either $\alpha_1\beta_2\gamma_{2S}$ or $\alpha_3\beta_3\gamma_{2S}$ channels by

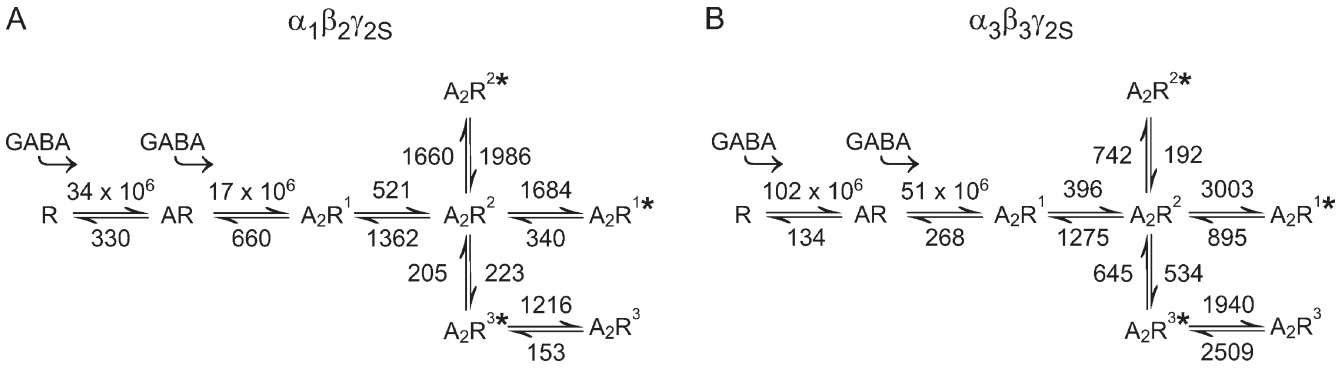

Figure 7. Proposed mechanism for $GABA_A$ receptor activation. Reaction schemes obtained from global fitting data across a range of GABA concentrations for $\alpha_1\beta_2\gamma_{2S}$ $GABA_A$ receptors (A) and $\alpha_3\beta_3\gamma_{2S}$ $GABA_A$ receptors (B). The mean forward and backward rate constants are indicated on either side of the double arrows between each of the states. Note the difference in binding rate constants (k_{-1} and k_{+1}) and backward rate constant (σ_{-1}) from A_2R^3 to A_2R^{3*} and the similarity in the flipping constants (φ_{-1} and φ_{+1}) between the two channels.

TABLE V

Equilibrium constants for activation of $\alpha_1\beta_2\gamma_{2S}$ and $\alpha_3\beta_3\gamma_{2S}$ $GABA_A$ receptors using Scheme 1

	$K_d = k_{-1}/k_{+1}$ (μM)	$\Phi = \phi_{+1}/\phi_{-1}$	$E_1 = \beta_1/\alpha_1$	$E_2 = \beta_2/\alpha_2$	$E_3 = \beta_3/\alpha_3$	$\Sigma = \sigma_{+1}/\sigma_{-1}$
$\alpha_1\beta_2\gamma_{2S}$	19.4	0.38	5.0	0.8	1.1	7.9
$\alpha_3\beta_3\gamma_{2S}$	2.63	0.31	3.4	3.9	0.8	0.8

rapid application of saturating concentrations of agonist. The 10–90% rise time and the deactivation time constants were determined for single-pulse responses, and the relative difference between peaks was determined for paired-pulse responses. Schemes 1, 2, and 4, along with mean rate constants, were used to simulate macropatch currents, also in response to a single or pairs of ultrafast agonist applications. These are shown in Fig. 8. As can be seen from comparisons of real and simulated current parameters, Schemes 1 and 4 recapitulated ensemble currents most accurately. Scheme 1 reproduced single-pulse deactivation kinetics and paired-pulse data best for the $\alpha_1\beta_2\gamma_{2S}$ channels. The simulated rise time was somewhat high and was improved by increasing φ_{+1} to 1,250 s^{-1}, but at the expense of the other parameters. Scheme 4 produced a slow activation rate and inadequate deactivation and paired-pulse values. For the $\alpha_3\beta_3\gamma_{2S}$ channels, Schemes 1 and 4 were more difficult to distinguish. Both produced activation rates and paired-pulse peaks that were similar to the real currents. The literature produced a wide range of deactivation parameters, but our simulated currents were most similar to IPSCs and excised patch currents recorded by Schofield and Huguenard (2007).

DISCUSSION

This study was undertaken with two complementary aims. We first wished to characterize the $\alpha_1\beta_1\gamma_{2S}$ and $\alpha_3\beta_3\gamma_{2S}$ $GABA_A$ receptors by measuring single-channel properties, such as i-V relationships, conductance, cluster duration, and intraburst P_O so as to better understand the differences in IPSCs mediated by the two channels. Second, we also wished to derive a plausible activation mechanism for the $GABA_A$ receptor that was more comprehensive than our previous attempt (Keramidas and Harrison, 2008) by including agonist-binding steps and by applying a full mechanism to two channel isoforms. This also enabled us to express the observed differences between the two channels within the framework of a mechanism and rate constants.

Single-channel conductance and i-V relationships

The first series of experiments was undertaken to yield information about some straightforward single-channel

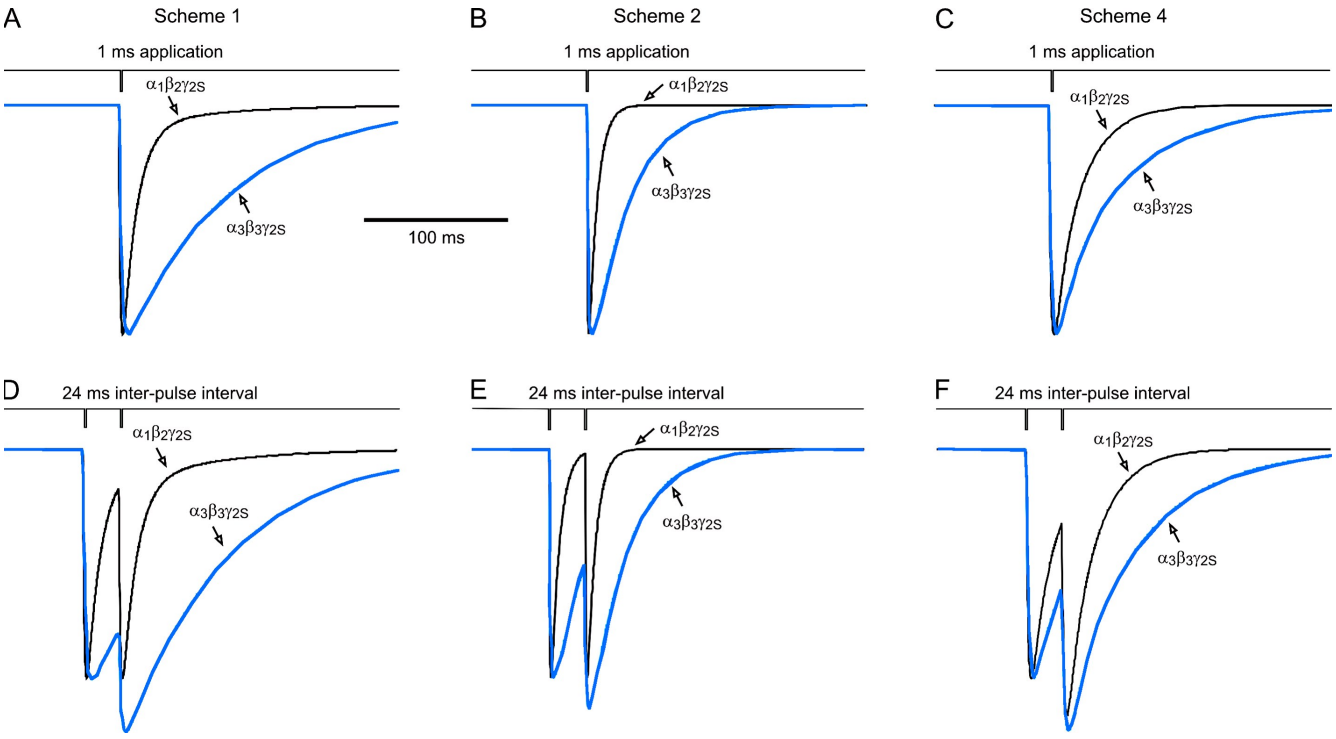

Figure 8. Simulated ensemble currents. Current simulations generated by Schemes 1, 2, and 4 for the $\alpha_1\beta_2\gamma_{2S}$ $GABA_A$ receptors (black) and $\alpha_3\beta_3\gamma_{2S}$ $GABA_A$ receptors (blue). (A–C) Simulated response to a 1-ms application of agonist. (D–F) Simulated responses to a pair of agonist applications, separated by 24 ms.

TABLE VI

Simulated versus experimental ensemble current parameters

Channel	Mechanism	10–90% RT (ms)	Deactivation				PP (% of first peak)
			τ_1 (ms)	A_1	τ_2 (ms)	A_2	
$\alpha_1\beta_2\gamma_{2S}$	S1	1.07	10.0	0.90	89.0	0.10	98
	S1 (φ_{+1} = 1,250)	0.96	12.6	0.84	75.6	0.16	92
	S2	0.20	5.77	0.44	–	–	99
	S4	1.35	7.85	0.22	21.1	0.78	116
	Experimental	0.65[a]	8.60 ± 0.81[b]	0.91± 0.01[b]	88.3 ± 4.7[b]	0.09 ± 0.02[b]	0.96 ± 0.04[c]
$\alpha_3\beta_3\gamma_{2S}$	S1	1.65	72.2	0.98	229	0.02	123
	S2	0.84	25.4	0.98	101	0.02	113
	S4	1.53	14.2	0.23	52.6	0.77	123
	Experimental	1.60 ± 0.28[d]	∼10–70[e]	∼0.45[e]	∼170–450[e]	∼0.55[e]	122[f]

[a]Interpolated from activation plot at 5 mM GABA in Keramidas and Harrison (2008).
[b]n = 6.
[c]24-ms interpulse interval; n = 16.
[d]At 5 mM GABA; n = 3.
[e]Values obtained from Mozrzymas et al. (2007) and Schofield and Huguenard (2007).
[f]25-ms interpulse interval (Schofield and Huguenard, 2007).
RT, rise time; PP, paired-pulse.

properties of $\alpha_1\beta_2\gamma_{2S}$ and $\alpha_3\beta_3\gamma_{2S}$ $GABA_A$ receptors. The two channels were similar in several respects. i-V relationships for both channels were comparable with little evidence for current rectification in either. Both channels exhibited a predominant high conductance (∼23–25 pS at −70 mV), which was only slightly higher in $\alpha_1\beta_2\gamma_{2S}$ $GABA_A$ receptors, and a less frequent small conductance of ∼14–15 pS. Active periods could be characterized in three ways in relation to conductance. They were either exclusive of the high (>80% of the activity) or low conductance, or they contained transitions from one to the other. The most observable case of transitions was the large conductance transitioning to the smaller for brief sojourns of ∼10–50 ms. The mechanism of multiple conductance states in ion channels is somewhat of an enigma, but there is now good evidence that in cys-loop channels it is regulated by the intracellular domain (Kelley et al., 2003; Hales et al., 2006; Carland et al., 2009). It is conceivable that the channels could achieve multiple conductance states by dynamically regulating the orientation of residues lining the intracellular conductance portals or the shape of the portals themselves.

Divergent properties of active periods of $\alpha_1\beta_2\gamma_{2S}$ and $\alpha_3\beta_3\gamma_{2S}$ $GABA_A$ receptors

We made measurements of the durations and open probabilities of bursts or clusters (intraburst P_Os). This analysis exposed significant differences between the two channel isoforms. The cluster/burst lengths of $\alpha_1\beta_2\gamma_{2S}$ $GABA_A$ receptors were consistently shorter at a given GABA concentration than the corresponding cluster/burst lengths for $\alpha_3\beta_3\gamma_{2S}$ $GABA_A$ receptors. At 5 mM GABA, which is close to the concentration reached at the synaptic cleft upon mass vesicular release of GABA (Mody et al., 1994), the cluster length of the $\alpha_1\beta_2\gamma_{2S}$ channels was ∼100 ms, approximately half that of $\alpha_3\beta_3\gamma_{2S}$ channels. Lema and Auerbach (2006) report cluster durations for the $\alpha_1\beta_1\gamma_{2S}$ isoform in the presence of 5 mM GABA to be ∼5–10 s, not the ∼100–200-ms cluster lengths estimated in this study for the $\alpha_1\beta_2\gamma_{2S}$ and $\alpha_3\beta_3\gamma_{2S}$ channels. The likely reason for the disparity is the consistently shorter t_{crit} values used in this study to isolate clusters. At 5 mM GABA, our clusters were defined by t_{crit} values that ranged between 8 and 20 ms, with a mean of ∼10 ms. In the Lema and Auerbach (2006) study, t_{crit} values were ≥15 ms and up to ∼60 ms.

At very low GABA concentrations (2 µM), which is the concentration reached at the synaptic cleft near the end of a synaptic event, the duration of bursts of $\alpha_1\beta_2\gamma_{2S}$ channel activity was ∼18 ms compared with ∼52 ms for the $\alpha_3\beta_3\gamma_{2S}$ channels. Indeed, the mean burst duration elicited by 20 µM GABA at $\alpha_1\beta_2\gamma_{2S}$ channels (∼46 ms) was closer to, but still shorter than, that evoked by 2 µM GABA at $\alpha_3\beta_3\gamma_{2S}$ channels, an order of magnitude difference in GABA. This property alone could to a significant degree account for the slower deactivation time course of IPSCs recorded in RTN (Schofield and Huguenard, 2007; Jia et al., 2009), as has been clearly shown for the deactivation phase of ensemble currents mediated by NMDA channels (Wyllie et al., 1998).

Another marked difference between the two channels was the divergent intraburst P_O as a function of decreasing GABA concentration. At 5 mM GABA, the P_O estimates were very similar for both channels, being 0.81 and 0.77. However, at 2 µM GABA, the difference in P_Os was substantial. For the $\alpha_1\beta_2\gamma_{2S}$ channels, the P_O was 0.16, whereas for the $\alpha_3\beta_3\gamma_{2S}$ channels, it was 0.45. This relatively high P_O of the later channels may also contribute to a slower rate of IPSC decay at RTN synapses,

as GABA is eliminated within the synaptic cleft. But it should be acknowledged that other factors may also play a role because the rate of active GABA clearance at the synaptic cleft is itself dependent on uptake mechanisms, as passive clearance is dependent on synaptic architecture, both of which could differ between VB and RTN synapses.

Global fitting of mechanisms across GABA concentrations

The second aim was achieved by global fitting of single-channel data recorded over a wide range of GABA concentrations, as has been done previously for glycine and muscle nACh receptors (Burzomato et al., 2004; Lape et al., 2008) and another subtype of $GABA_A$ receptor (Lema and Auerbach, 2006). Saturating GABA (5 mM) provided data for the gating portion of the mechanism and an initial means of reducing the number of potential schemes. The agonist-binding steps were determined with the addition of data recorded at below-saturating concentrations (200 µM and 20 or 2 µM).

Generating dwell histograms for the high, intermediate, and low concentration data revealed a general pattern in the time constants of the individual exponential components. Three open components and three or four shut components were required to adequately fit the data from both channels, in agreement with other studies on $GABA_A$ receptors (Steinbach and Akk, 2001; Lema and Auerbach, 2006). Dwell-time distribution components (time constants and fractions) collectively determine the rate constants for transitions between channel states in postulated mechanisms, but in a complex and mechanism-dependent manner (Colquhoun and Hawkes, 1995; Shelley and Magleby, 2008). To understand better how the differences in burst properties between the two channels are achieved, we need to refer to the fitted schemes. Our mechanisms are consistent with the observed longer active periods in $\alpha_3\beta_3\gamma_{2S}$ receptors. 20 mechanisms were evaluated, including the best scheme obtained from cell-attached patch recordings of $\alpha_1\beta_1\gamma_{2S}$ $GABA_A$ receptors (Scheme 2; Lema and Auerbach, 2006) and a scheme proposed for the muscle nACh receptor (Lape et al., 2008) that we modified to included three conducting states (Scheme 3). Other schemes that included loops were not considered. Of the schemes we did test, the one that fit the data most consistently and with the highest ΣLL values was Scheme 1. Scheme 2 also fit the datasets adequately, whereas Scheme 3 generally failed to properly fit most of the datasets. Scheme 4 was statistically very similar to Scheme 1. This scheme features two sequential open states and an intermediate shut state preceding the third open state.

Simulations of macropatch currents

So as not to be exclusively reliant on LL fitting of single-channel data, we simulated macropatch currents using Schemes 1, 2, and 4 along with optimized rate constants as an independent means of ranking schemes. Simulations of single- and double-pulse currents were then compared with real currents for both channel isoforms. Consistent with the single-channel burst analysis, Scheme 1 generated currents that most closely resembled real currents in terms of activation, deactivation, and paired-pulse peak measurements for both channels. None of the schemes reproduced all the measured macropatch parameters for both channels. For instance, Scheme 1 reproduced the deactivation time constants and paired-pulse peak values well for the $\alpha_1\beta_2\gamma_{2S}$ channels, but it gave an activation rate that was 1.6 times slower than the measured rate. However, we do not regard this shortcoming as a major drawback of the scheme. Nevertheless, in an attempt to reduce the activation rate, we manually varied some of the rate constants and found that increasing φ_{+1} had the desired effect, but this perturbed the other values. For the $\alpha_3\beta_3\gamma_{2S}$ channels, Scheme 1 successfully reproduced the activation rate and the paired-pulse peak currents. The deactivation time constants were also in reasonable agreement with the real data, but the fractions were less so. It was also difficult to find consistent deactivation data in the literature for this channel.

The simulations provided good corroborative evidence that Scheme 1 is the overall best mechanism for channel activation. The result that single-channel analysis and macropatch data both favor Scheme 1, albeit only marginally and for two kinetically different $GABA_A$ receptors, suggest that this scheme is a sufficient general mechanism that could form the basis for further $GABA_A$ receptor kinetic studies.

Interpretations and caveats

In our efforts to develop an activation mechanism for the $GABA_A$ receptor, we simplified the analysis by omitting low conductance activity, even though it is clearly present in both channel isoforms, either on its own or as sojourns from the high conductance openings. Indeed, $GABA_A$ receptor single-channel sublevels have been known for considerable time (Hamill et al., 1983). As we removed all (or most) of the low conductance activity, our schemes describe only activation to high conductance activity, and in this regard our mechanism(s) can only be partial. We know of no modeling studies of cys-loop receptors that explicitly incorporate subconductance levels in the analysis. We hypothesize that the low conductance activity represents a distinct class of protein conformations, but we cannot here distinguish between intrinsic regulation of low conductance states, as might occur by dynamic changes in conformation of the intracellular conductance portals and extrinsic effects, such as channel block by ions in solution. This indeed applies to any state in our mechanism. The notion that channel activation occurs as a "conformational

wave" in the muscle nACh receptor (Grosman et al., 2000; Purohit et al., 2007) is consistent with classes of functional (open or shut or conductance) states in cys-loop channels being intrinsic properties of the channels. However, it has been demonstrated convincingly that fast-channel block in the muscle-type nACh receptor by organic cations effectively diminished channel conductance (Akk and Steinbach, 2003; Lape et al., 2008, 2009). These studies also show that channel block does not necessarily have to occur from open states, and that shut channels can trap the blocking agent, producing discrete shut states. It is not clear from this study whether the states (open, shut, or conductance) arise due to intrinsic properties of the channel or are induced extrinsically. For instance, our investigations found that one of the primary kinetic differences between the two $GABA_A$ receptor isoforms was the transition between an open state (A_2R^3*) and a shut state (A_2R^3), and we infer that the A_2R^3 state is essentially similar in both channel isoforms but shorter lived in the $\alpha_3\beta_3\gamma_{2S}$ channels. However, we cannot distinguish between A_2R^3 being intrinsically less stable or preferentially destabilized in the $\alpha_3\beta_3\gamma_{2S}$ channels by solutes (e.g., Mg^{2+}) or if A_2R^3* is simply blocked by ions in the $\alpha_1\beta_2\gamma_{2S}$ channels, manifesting as A_2R^3. The similarity in the i-Vs of both channel isoforms leads us, however, to strongly favor intrinsic instability of the third shut state in the $\alpha_3\beta_3\gamma_{2S}$ channels on the basis of subunit differences rather than a supposed modulation by ions.

Although our analysis favored Scheme 1 over Schemes 4 and 2, it should be pointed out that there are some common features between the three schemes. All have three open and three shut diliganded states and connect the first diliganded shut state to a second before channel opening occurs. The entry into preconducting states after agonist binding is also a critical feature of Scheme 3, the original form of which was applied to the muscle nACh receptor and elucidates the mechanism of partial agonism (Lape et al., 2008). Liganded preconducting states, coined "flipped" or "primed," have been demonstrated in several cys-loop receptors, including glycine receptors (Burzomato et al., 2004; Lape et al., 2008), muscle ACh receptors (Lape et al., 2008; Mukhtasimova et al., 2009), and $GABA_A$ receptors (Lema and Auerbach, 2006; Keramidas and Harrison, 2008). Preconducting states have also been identified in other ligand-gated ion channels that are not closely related to the cys-loop family. Using partial agonists as substitutes for either glycine or glutamate at NMDA receptors composed of NR1 and NR2B subunits revealed subunit-specific conformational transitions involving either the NR1 or NR2B before channel opening (Banke and Traynelis, 2003). Kinetic studies of $P2X_2$-mediated macroscopic currents have provided evidence of a lag in time between ligand binding and the detection of current. These data were modeled accurately with schemes that included fully liganded shut states that preceded the opening of the channel (Moffatt and Hume, 2007).

The main difference between Schemes 1, 2, and 4 in this study is the connectivity of the fully liganded states. With regard to Schemes 1 and 2, if we assume that both schemes accurately account for the respective data they are applied to, we can only speculate as to why the schemes are different, even though they both fit $GABA_A$ receptor single-channel data recorded across high and low GABA concentrations using essentially the same analysis method. Scheme 2 was determined for data obtained in the cell-attached configuration, where the channels are exposed to intracellular solutes, including ions that affect channel kinetics, such as Ca^{2+} and Cl^- (Fucile et al., 2000; Pitt et al., 2008). Pitt et al. (2008) show that low intracellular Cl^-, as is present in intact cells, slows ensemble current deactivation and alters the rate constants and potentially the states in the underlying scheme in glycine receptors, which are close Cl^--selective cousins of $GABA_A$ receptors. It has also been shown that kinetics of $GABA_A$ receptors expressed in HEK293 cells are substantially affected by the extent of phosphorylation by protein kinase A (Hinkle and Macdonald, 2003). It is conceivable that patch excision alters the constitutive phosphorylation state of the channels, impacting on their kinetic behavior.

To facilitate a comparison of the activation properties of the two channels, the equilibrium constants (ratio of forward and backward rate constants) were computed (Table V). From these numbers it can be deduced that the tendency toward the conducting states (A_2R^n*) between the two channels differs (E_1, E_2, and E_3) by only two- to fivefold. Notably, the equilibrium constant for the diliganded preconducting state (Φ, or the "flipping" or "priming" constant) is essentially the same for both channels ($\sim$0.3–0.4) and not very different to that determined for $\alpha_1\beta_1\gamma_{2S}$ $GABA_A$ receptors (Lema and Auerbach, 2006). It would be informative to investigate if other agonists, such as muscimol and piperidine-4 sulphonic acid (P4S) affect Φ, as might be predicted by the Lape et al. (2008) study. The most evident differences between the channels is the GABA-binding reaction (K_d) and the transition between the open and shut states, A_2R^{3*} and A_2R^3 (Σ). Lema and Auerbach (2006) report a K_d value of 91 µM, which is dissimilar to the values determined in this study. According to our estimates, GABA binds to the $\alpha_3\beta_3\gamma_{2S}$ $GABA_A$ receptor (K_d = 2.62) with an over sevenfold higher affinity for GABA than $\alpha_1\beta_2\gamma_{2S}$ $GABA_A$ receptors (K_d = 19.4). We suggest that this would tend to favor the right-hand or gating part of mechanism and consequently lengthen the active periods. Moreover, Σ is about an order of magnitude smaller for the $\alpha_3\beta_3\gamma_{2S}$ receptors (A_2R^3 has shorter lifetime), which would also account for the higher P_O of these channels at most GABA concentrations tested. Collectively,

these kinetic effects are consistent with observed differences in deactivation of IPSCs of RTN synapses compared with those of VB. Our estimates of K_d obtained from Scheme 1 for the $\alpha_1\beta_2\gamma_{2S}$ channels are relatively low compared with that found by Lema and Auerbach (2006) for the closely related $\alpha_1\beta_1\gamma_{2S}$ receptor. Schemes 2 and 4 yielded K_ds that were more comparable, being 132 and 96 µM, respectively. We can offer several plausible reasons for the discrepancy in K_ds. First, it is apparent from our analysis that the estimate of K_d is mechanism dependent, and that the $\alpha_1\beta_2\gamma_{2S}$ the $\alpha_1\beta_1\gamma_{2S}$ channels were described by different schemes. If we compare K_ds computed from the same scheme (Scheme 2), the difference in affinity between the $\alpha_1\beta_2\gamma_{2S}$ and $\alpha_1\beta_1\gamma_{2S}$ channels is reduced from 4.7- to 1.1-fold. Another potential reason for the discrepant K_ds between the $\alpha_1\beta_2\gamma_{2S}$ and $\alpha_1\beta_1\gamma_{2S}$ channels is the choice of t_{crit} values between this study and that of Lema and Auerbach (2006). It is conceivable that relatively short t_{crit} values used in this study, especially for the data at 20 and 2 µM GABA, led to inadvertently omitting some long binding events that are longer than t_{crit}. This would result in underestimating K_d. However, when we varied t_{crit} from 35 to 100 ms in two patches recorded at 2 µM GABA, we found no difference in the computed K_d for either patch. It should also be emphasized that the different K_ds may reflect a real difference in affinity between the $\alpha_1\beta_2\gamma_{2S}$ and $\alpha_1\beta_1\gamma_{2S}$ channels, conferred by different amino acid sequences at critical binding segments. The β subunit contributes three components to the GABA-binding pocket. One of these is the crucial loop 10-β sheet 10-segment or "loop C" (Kash et al., 2004). An alignment of these segments reveals a difference in primary sequence at two positions between the β_2 and β_1 subunits.

The complication of affinity estimates obtained via different mechanisms is avoided with respect to the different K_ds between the $\alpha_1\beta_2\gamma_{2S}$ and $\alpha_3\beta_3\gamma_{2S}$ channels, which we hypothesize reflect different binding site affinities. Alignments of homologous segments that form the GABA-binding pocket between the β–α subunit interfaces reveal a total of 11 amino acids that differ between the two channels. Ultimately, site-directed mutations and a reanalysis using the same mechanism will aid in verifying the K_ds and determining the underlying factors for the apparent affinity differences between the $\alpha_1\beta_1\gamma_{2S}$, $\alpha_1\beta_2\gamma_{2S}$, and $\alpha_3\beta_3\gamma_{2S}$ channels.

Conclusion

We have constructed and tested a potential reaction mechanism that provides an adequate description of the kinetic behavior of two major subtypes of the $GABA_A$ receptor and explains why inhibitory synaptic currents are much longer lasting at synapses containing one subtype than the other. The model incorporates preconducting states that are apparently a conserved feature of the family of cys-loop receptors. Future efforts will be directed toward the application of this mechanism to additional $GABA_A$ receptor subtypes and evaluation of the effects of a variety of pharmacological challenges, including agonists, partial agonists, and modulators, such as benzodiazepines and general anaesthetics.

This work was supported by National Institutes of Health (grant AA016393).

Angus C. Nairn served as editor.

Submitted: 17 August 2009
Accepted: 11 December 2009

REFERENCES

Akk, G., and J.H. Steinbach. 2003. Activation and block of mouse muscle-type nicotinic receptors by tetraethylammonium. *J. Physiol.* 551:155–168. doi:10.1113/jphysiol.2003.043885

Auerbach, A. 2005. Gating of acetylcholine receptor channels: brownian motion across a broad transition state. *Proc. Natl. Acad. Sci. USA.* 102:1408–1412. doi:10.1073/pnas.0406787102

Banke, T.G., and S.F. Traynelis. 2003. Activation of NR1/NR2B NMDA receptors. *Nat. Neurosci.* 6:144–152. doi:10.1038/nn1000

Barberis, A., J.W. Mozrzymas, P.I. Ortinski, and S. Vicini. 2007. Desensitization and binding properties determine distinct α1β2γ2 and α3β2γ2 GABA(A) receptor-channel kinetic behavior. *Eur. J. Neurosci.* 25:2726–2740. doi:10.1111/j.1460-9568.2007.05530.x

Burzomato, V., M. Beato, P.J. Groot-Kormelink, D. Colquhoun, and L.G. Sivilotti. 2004. Single-channel behavior of heteromeric α1β glycine receptors: an attempt to detect a conformational change before the channel opens. *J. Neurosci.* 24:10924–10940. doi:10.1523/JNEUROSCI.3424-04.2004

Carland, J.E., M.A. Cooper, S. Sugiharto, H.J. Jeong, T.M. Lewis, P.H. Barry, J.A. Peters, J.J. Lambert, and A.J. Moorhouse. 2009. Characterization of the effects of charged residues in the intracellular loop on ion permeation in α1 glycine receptor channels. *J. Biol. Chem.* 284:2023–2030. doi:10.1074/jbc.M806618200

Colquhoun, D., and A.G. Hawkes. 1995. The principles of the stochastic interpretation of ion-channel mechanisms. *In* Single-Channel Recordings. 2nd Edition. Plenum Press, NY. 397–482 pp.

Colquhoun, D., C.J. Hatton, and A.G. Hawkes. 2003. The quality of maximum likelihood estimates of ion channel rate constants. *J. Physiol.* 547:699–728. doi:10.1113/jphysiol.2002.034165

Farrant, M., and Z. Nusser. 2005. Variations on an inhibitory theme: phasic and tonic activation of GABA(A) receptors. *Nat. Rev. Neurosci.* 6:215–229. doi:10.1038/nrn1625

Fucile, S., D. De Saint Jan, L.P. de Carvalho, and P. Bregestovski. 2000. Fast potentiation of glycine receptor channels of intracellular calcium in neurons and transfected cells. *Neuron.* 28:571–583. doi:10.1016/S0896-6273(00)00134-3

Grosman, C., M. Zhou, and A. Auerbach. 2000. Mapping the conformational wave of acetylcholine receptor channel gating. *Nature.* 403:773–776. doi:10.1038/35001586

Hales, T.G., J.I. Dunlop, T.Z. Deeb, J.E. Carland, S.P. Kelley, J.J. Lambert, and J.A. Peters. 2006. Common determinants of single channel conductance within the large cytoplasmic loop of 5-hydroxytryptamine type 3 and α4β2 nicotinic acetylcholine receptors. *J. Biol. Chem.* 281:8062–8071. doi:10.1074/jbc.M513222200

Hamill, O.P., J. Bormann, and B. Sakmann. 1983. Activation of multiple-conductance state chloride channels in spinal neurones by glycine and GABA. *Nature.* 305:805–808. doi:10.1038/305805a0

Hinkle, D.J., and R.L. Macdonald. 2003. β subunit phosphorylation selectively increases fast desensitization and prolongs deactivation of α1β1γ2L and α1β3γ2L GABA(A) receptor currents. *J. Neurosci.* 23:11698–11710.

Jia, F., P.A. Goldstein, and N.L. Harrison. 2009. The modulation of synaptic GABA(A) receptors in the thalamus by eszopiclone and zolpidem. *J. Pharmacol. Exp. Ther.* 328:1000–1006. doi:10.1124/jpet.108.146084

Jones, M.V., and G.L. Westbrook. 1995. Desensitized states prolong GABAA channel responses to brief agonist pulses. *Neuron.* 15:181–191. doi:10.1016/0896-6273(95)90075-6

Kash, T.L., J.R. Trudell, and N.L. Harrison. 2004. Structural elements involved in activation of the γ-aminobutyric acid type A (GABAA) receptor. *Biochem. Soc. Trans.* 32:540–546. doi:10.1042/BST0320540

Kelley, S.P., J.I. Dunlop, E.F. Kirkness, J.J. Lambert, and J.A. Peters. 2003. A cytoplasmic region determines single-channel conductance in 5-HT3 receptors. *Nature.* 424:321–324. doi:10.1038/nature01788

Keramidas, A., and N.L. Harrison. 2008. Agonist-dependent single channel current and gating in $\alpha_4\beta_2\delta$ and $\alpha_1\beta_2\gamma_{2S}$ $GABA_A$ receptors. *J. Gen. Physiol.* 131:163–181. doi:10.1085/jgp.200709871

Kienker, P. 1989. Equivalence of aggregated Markov models of ion-channel gating. *Proc. R. Soc. Lond. B Biol. Sci.* 236:269–309. doi:10.1098/rspb.1989.0024

Krasowski, M.D., and N.L. Harrison. 1999. General anaesthetic actions on ligand-gated ion channels. *Cell. Mol. Life Sci.* 55:1278–1303. doi:10.1007/s000180050371

Lape, R., D. Colquhoun, and L.G. Sivilotti. 2008. On the nature of partial agonism in the nicotinic receptor superfamily. *Nature.* 454:722–727.

Lape, R., P. Krashia, D. Colquhoun, and L.G. Sivilotti. 2009. Agonist and blocking actions of choline and tetramethylammonium on human muscle acetylcholine receptors. *J. Physiol.* 587:5045–5072. doi:10.1113/jphysiol.2009.176305

Lee, W.Y., C.R. Free, and S.M. Sine. 2009. Binding to gating transduction in nicotinic receptors: Cys-loop energetically couples to pre-M1 and M2-M3 regions. *J. Neurosci.* 29:3189–3199. doi:10.1523/JNEUROSCI.6185-08.2009

Lema, G.M., and A. Auerbach. 2006. Modes and models of GABA(A) receptor gating. *J. Physiol.* 572:183–200.

Mody, I., and R.A. Pearce. 2004. Diversity of inhibitory neurotransmission through GABA(A) receptors. *Trends Neurosci.* 27:569–575. doi:10.1016/j.tins.2004.07.002

Mody, I., Y. De Koninck, T.S. Otis, and I. Soltesz. 1994. Bridging the cleft at GABA synapses in the brain. *Trends Neurosci.* 17:517–525. doi:10.1016/0166-2236(94)90155-4

Moffatt, L., and R.I. Hume. 2007. Responses of rat $P2X_2$ receptors to ultrashort pulses of ATP provide insights into ATP binding and channel gating. *J. Gen. Physiol.* 130:183–201. doi:10.1085/jgp.200709779

Mozrzymas, J.W., A. Barberis, and S. Vicini. 2007. GABAergic currents in RT and VB thalamic nuclei follow kinetic pattern of α3- and α1-subunit-containing GABAA receptors. *Eur. J. Neurosci.* 26:657–665. doi:10.1111/j.1460-9568.2007.05693.x

Mukhtasimova, N., W.Y. Lee, H.L. Wang, and S.M. Sine. 2009. Detection and trapping of intermediate states priming nicotinic receptor channel opening. *Nature.* 459:451–454. doi:10.1038/nature07923

Olsen, R.W., and W. Sieghart. 2008. International Union of Pharmacology. LXX. Subtypes of gamma-aminobutyric acid(A) receptors: classification on the basis of subunit composition, pharmacology, and function. Update. *Pharmacol. Rev.* 60:243–260. doi:10.1124/pr.108.00505

Pitt, S.J., L.G. Sivilotti, and M. Beato. 2008. High intracellular chloride slows the decay of glycinergic currents. *J. Neurosci.* 28:11454–11467. doi:10.1523/JNEUROSCI.3890-08.2008

Purohit, P., A. Mitra, and A. Auerbach. 2007. A stepwise mechanism for acetylcholine receptor channel gating. *Nature.* 446:930–933. doi:10.1038/nature05721

Qin, F., A. Auerbach, and F. Sachs. 1996. Estimating single-channel kinetic parameters from idealized patch-clamp data containing missed events. *Biophys. J.* 70:264–280. doi:10.1016/S0006-3495(96)79568-1

Schofield, C.M., and J.R. Huguenard. 2007. GABA affinity shapes IPSCs in thalamic nuclei. *J. Neurosci.* 27:7954–7962. doi:10.1523/JNEUROSCI.0377-07.2007

Shelley, C., and K.L. Magleby. 2008. Linking exponential components to kinetic states in Markov models for single-channel gating. *J. Gen. Physiol.* 132:295–312. doi:10.1085/jgp.200810008

Sieghart, W., and G. Sperk. 2002. Subunit composition, distribution and function of GABA(A) receptor subtypes. *Curr. Top. Med. Chem.* 2:795–816. doi:10.2174/1568026023393507

Steinbach, J.H., and G. Akk. 2001. Modulation of GABA(A) receptor channel gating by pentobarbital. *J. Physiol.* 537:715–733. doi:10.1113/jphysiol.2001.012818

Wagner, D.A., C. Czajkowski, and M.V. Jones. 2004. An arginine involved in GABA binding and unbinding but not gating of the GABA(A) receptor. *J. Neurosci.* 24:2733–2741. doi:10.1523/JNEUROSCI.4316-03.2004

Wyllie, D.J., P. Béhé, and D. Colquhoun. 1998. Single-channel activations and concentration jumps: comparison of recombinant NR1a/NR2A and NR1a/NR2D NMDA receptors. *J. Physiol.* 510:1–18. doi:10.1111/j.1469-7793.1998.001bz.x